Inactivating BK Channels in Rat Chromaffin Cells May Arise from Heteromultimeric Assembly of Distinct Inactivation-Competent and Noninactivating Subunits

J. P. Ding, Z. W. Li, and C. J. Lingle
Department of Anesthesiology, Washington University School of Medicine, St. Louis, Missouri 63110 USA

ABSTRACT Inactivating and noninactivating variants of large-conductance, Ca^{2+}-dependent, voltage-dependent BK-type channels are found in rat chromaffin cells and are largely segregated into different cells. Here we test the hypothesis that, within the population of cells that express inactivating BK current (BK_i current), the BK_i channels are largely heteromultimers composed of inactivation-competent subunits (bk_i) and noninactivating subunits (bk_s). Several independent types of evidence support this view. The gradual removal of inactivation by trypsin is consistent with the idea that in most cells and patches there are, on average, about two to three inactivation domains per channel. In addition, several aspects of blockade of BK_i current by charybdotoxin (CTX) are consistent with the idea that BK_i channels contain differing numbers (one to four) of relatively CTX-resistant bk_i subunits. Finally, the frequency of occurrence of noninactivating BK_s channels in patches with predominantly inactivating BK_i channels is consistent with the binomial expectations of random, independent assembly of two distinct subunits, if most cells have, on average, about two to three bk_i subunits per channel. These results suggest that the phenotypic properties of BK_i currents and the resulting cellular electrical excitability may exhibit a continuum of behavior that arises simply from the differential expression of two distinct subunits.

INTRODUCTION

Rat adrenal chromaffin cells maintained in primary cell culture express either of two phenotypic forms of large-conductance, Ca^{2+}-dependent, voltage-dependent K^+ channel (BK-type). One form, termed BK_i, exhibits rapid and essentially complete inactivation after activation, whereas the other, termed BK_s, exhibits the more usual sustained activation (Solaro and Lingle, 1992; Solaro et al., 1995). In those cells and patches that express BK_i channels (~80%), there appears to be little or no Ca^{2+}-dependent and voltage-dependent current that is noninactivating.

Despite the segregation of inactivating and noninactivating BK current phenotypes among chromaffin cells, some aspects of the behavior of BK_i current have suggested that BK_i channels may not be homogeneous. First, among cells and patches exhibiting complete BK current inactivation, there is some variability in limiting inactivation rates (Solaro et al., 1995, 1997). Second, we have noted that BK_i currents exhibit unexplained variability in sensitivity to charybdotoxin (CTX), whereas BK_s currents have the more usual CTX sensitivity (Solaro et al., 1995). Third, trypsin results in a gradual slowing of the BK_i inactivation rate, but in initial experiments the magnitude of this slowing was often less than would be expected from the hypothesis that BK channels contain four independent inactivation domains (Lingle et al., 1996). In addition, although the structural component of BK_i channels that confers inactivating behavior has not been identified, at least two alternative splice variants of *Slo* are found in chromaffin cells (Saito et al., 1997). Because of the known ability of members of the voltage-dependent K^+ channel superfamily to form heteromultimeric tetramers within their immediate subfamily (Covarrubias et al., 1991; Li et al., 1992), it would not be surprising to learn that different naturally occurring *Slo* splice variants have the ability to form heteromultimers.

Here we test the possibility that BK_i currents and channels arise from heteromultimeric expression of two subunits, one necessary to confer inactivation and the other responsible for CTX sensitivity. First, we examine the peptidase dependence of the onset and recovery from inactivation. These results support the idea that BK_i channels contain up to four independently acting inactivation domains, but that, on average, most channels contain less than four such domains. Second, the resistance of BK_i current to blockade by CTX is examined and found to correlate with the inactivation behavior of the current. Third, the frequency of occurrence of BK_s channels in patches with BK_i channels, although rare, is found to be consistent with the idea that, on average, BK channels contain two to three inactivation-competent subunits. The results support the hypothesis that phenotypic diversity in BK channels in rat chromaffin cells may arise in part from the heteromultimeric assembly of two distinct BK subunits.

Received for publication 21 July 1997 and in final form 25 September 1997.

Address reprint requests to Dr. Chris Lingle, Department of Anesthesiology, Washington University School of Medicine, 660 S. Euclid Ave., St. Louis, MO 63110. Tel.: 314-362-8558; Fax: 314-362-8571; E-mail: clingle@morpheus.wustl.edu.

0006-3495/98/01/268/22 $2.00

MATERIALS AND METHODS

Chromaffin cell culture

Methods of rat chromaffin cell isolation and maintenance of cultures were as described in previous work (Neely and Lingle, 1992a; Herrington et al.,

1995; Solaro et al., 1995) based on the procedures of others (Fenwick et al., 1978; Kilpatrick et al., 1980; Role and Perlman, 1980; Livett, 1984).

Electrophysiological methods

Whole-cell and single-channel currents were recorded with standard techniques (Hamill et al., 1981) as reported previously (Solaro and Lingle, 1992; Solaro et al., 1995; Neely and Lingle, 1992a,b; Herrington et al., 1995). In whole-cell experiments, uncompensated series resistance (R_s) was typically 1.5–5 MΩ, of which 80–95% was electronically compensated. Values for R_s and the percentage compensation for specific experiments are provided in the figure legends.

Solutions

The usual extracellular solution contained the following (in mM): 140 NaCl, 5.4 KCl, 10 HEPES, 1.8 $CaCl_2$, and 2.0 $MgCl_2$ (pH 7.4), adjusted with *N*-methylglucamine (NMG). When BK current was recorded with elevated pipette Ca^{2+}, the extracellular solution bathing the cell contained (in mM): 150 NaCl, 5.4 KCl, 4 $MgCl_2$, 10 HEPES, adjusted to pH 7.4 with NaOH. For whole-cell recording, the pipette solution contained the following (in mM): 160 KCl, 10 HEPES, 10 mM HEDTA with added Ca^{2+} to make 10 μM free Ca^{2+}, as defined by the EGTAETC program (E. McCleskey, Vollum Institute), with pH adjusted to 7.0. In some cases, KCl was partially removed by equimolar substitution of NaCl and/or CsCl to reduce the magnitude of the BK current. Trypsin (porcine pancreatic type IX; Sigma) was used in the pipette solution at 0.5 mg/ml. For experiments with trypsin, the tip of the pipette was first filled with the normal 10 μM Ca^{2+} solution, and then backfilled with the pipette solution containing trypsin. After formation of a gigaohm seal, whole-cell recording was not initiated for at least 7 min. At this time, the concentration of trypsin in the tip is at least 90% of that backfilled into the pipette (Pusch and Neher, 1988).

Osmolarity was measured by dew point (Wescor Osmometer) and adjusted to within 3% (internal saline, 290; external saline: 305). Apamin (200 nM) and 4-aminopyridine (4-AP) (1 mM) were routinely added to extracellular solutions to minimize contamination by SK currents (Neely and Lingle, 1992a) and voltage-dependent K^+ current, respectively. Tetrodotoxin (200 nM) was used to reduce voltage-dependent Na^+ current. For whole-cell recordings, no correction was made for the less than +3 mV liquid junction potential that arose when chloride-based salines were used for introducing high [Ca^{2+}] into cells.

For recordings of channel activity in patches, cells were bathed in the extracellular saline used for whole-cell recordings. Just before patch excision, the solution bathing the cell was changed to the 0 Ca^{2+} saline described below. For inside-out single-channel recordings, the pipette saline contained (in mM) 140 KCl, 20 KOH, 2 $MgCl_2$, 10 HEPES (pH 7.0), adjusted with 1 N HCl. Apamin (200 nM) was also included in the pipette solution. The cytosolic saline used during excised inside-out patch recordings was the following (in mM): 140 KCl, 20 KOH, 10 HEPES, 5 *N*-hydroxyethylethylene-diaminetriacetic acid (HEDTA), with added $CaCl_2$ to make 10 μM free [Ca^{2+}], with pH 7.0, adjusted with 1 N HCl. Estimates of free [Ca^{2+}] were determined as described previously (Solaro and Lingle, 1992; Herrington et al., 1995).

Solution exchange and drug applications were accomplished as described previously (Herrington et al., 1995). Chemicals were from Aldrich or Sigma.

Data analysis

Whole-cell and single-channel currents were analyzed either with Clampfit or with our own software. Currents or extracted data were fitted with a Levenberg-Marquardt search algorithm to obtain nonlinear least-squares estimates of function parameters. Modeling of current waveforms based on different subunit compositions was carried out with our software or, in some cases, with Mathcad (MathSoft, Cambridge, MA).

Estimates of drug dissociation constants were made by fitting the complete time course of blockade at one or more drug concentrations to a first-order blocking reaction as described (Saito et al., 1997). If a reasonable period of recovery from drug application was achieved, blocking rate constants and the resulting K_d were tightly constrained, even by single applications of drug. In cases where different concentrations of toxin were applied sequentially with no period of washout, the entire time course of block was fit as above, while making allowance for changes in the toxin concentration at appropriate times.

Estimates of τ_i versus f_{ss} and fitting of current waveforms

Current waveforms based on different binomial distributions of channel subunits were calculated with a Hodgkin-Huxley (1952) activation/inactivation model, assuming that channels of each stoichiometry activated with similar kinetics, but inactivated in accordance with the number of inactivation domains. Thus total current arose from the sum of currents through five different channel stoichiometries, with the fraction of channels of each type defined by a single parameter, the percentage bk_i subunits. For simulated currents, the activation time constant, τ_a, was 2.5 ms, with a cooperativity factor of 1.0, which is similar to values obtained directly from fitting whole-cell current waveforms in these cells (e.g., Fig. 14). The minimum time constant of inactivation (τ_{min}) for a channel with four inactivation domains was assumed to be 25 ms. The inactivation rate for a particular channel stoichiometry was directly proportional to the number of inactivation domains (the number of bk_i subunits). The CTX sensitivity of a particular channel stoichiometry was determined by the number of bk_s subunits, assuming a simple block model. The CTX dissociation rate was assumed to be independent of the number of bk_s subunits, and the association rate was assumed to scale with the number of bk_s subunits. A channel with four bk_s subunits was assumed to have a K_d for CTX block of 2 nM and a channel with four bk_i subunits to usually have a K_d of 100 nM. The simulated current waveform derived from particular binomial distributions was then fit with a standard Hodgkin-Huxley activation/inactivation model to define empirically the inactivation time constant and the amount of noninactivating current present at 300 ms in the waveform. Similarly, currents in the presence of CTX were calculated with the assumptions for toxin block given above. Although such simulated currents contain multiple exponential components in the current decay, a single exponential fit provides a reasonable approximation of the decay time course.

Fitting of actual current waveforms during the trypsin digestion process (Fig. 7) or before and after CTX application (Fig. 14) followed a similar strategy based on a binomial distribution of channels among five possible channel stoichiometries. A term for contaminating voltage-dependent current was also included (I_{KV}). In this procedure, if both I_{KV} and the percentage bk_i subunits are free parameters, resulting fits are not well defined. However, given particular assumptions as described in the Results, well-defined estimates of τ_{min} and percentage bk_i subunits under a given set of assumptions can be obtained.

Fitting of currents with either a standard Hodgkin-Huxley model or with an H-H model modified to include channels of differing stoichiometries used the entire current time course (e.g., Figs. 2, 6, 7, 14). Single exponential fits to inactivation time courses (e.g., Figs. 3, 5, 9) typically covered a range encompassing 80% to less than 2% of the peak amplitude of the decaying current. Estimates of τ_i with either method typically agreed within 1–2%.

RESULTS

A hypothesis to account for the diversity of BK current in rat chromaffin cells

Based on our preliminary results, we hypothesize that BK channels in chromaffin cells arise from two distinct BK subunits (Fig. 1):

1. an inactivation competent, CTX-resistant bk_i subunit

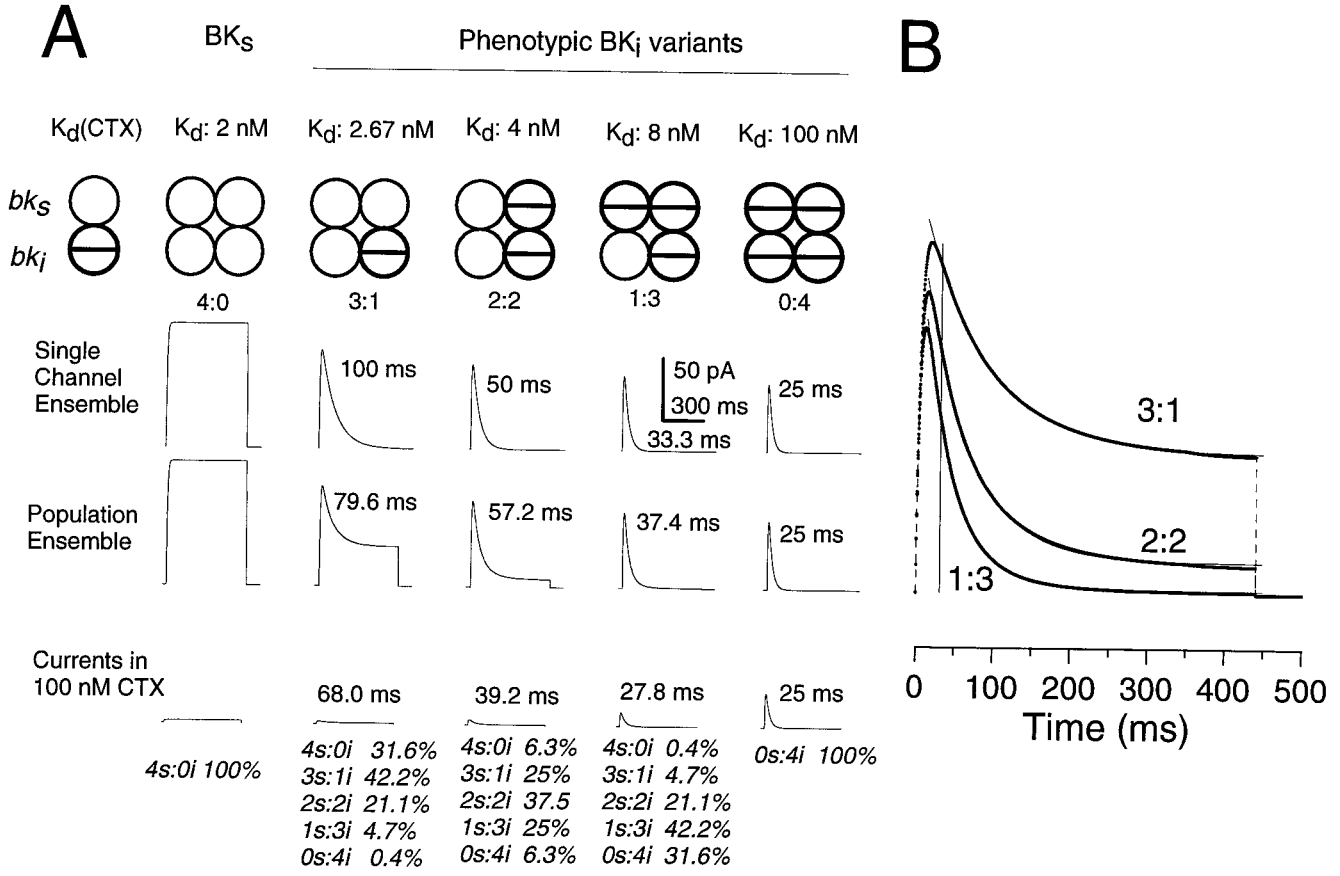

FIGURE 1 A model of BK channel assembly in chromaffin cells. (*A*) BK channels in chromaffin cells are proposed to arise from the random, independent assembly of two distinct BK subunits: an inactivation-competent, CTX-resistant bk_i subunit and an inactivation-null, CTX-sensitive bk_s subunit. Random assembly of subunits results in one BK_s single-channel phenotype and four BK_i phenotypes. Traces labeled Single Channel Ensemble reflect the average behavior of a single channel containing only the indicated ratios of bk_s:bk_i subunits. Traces labeled Population Ensemble reflect the behavior of a population of channels with the indicated average ratios of bk_s:bk_i subunits distributed binomially within the population. Macroscopic currents were generated assuming a 2.5-ms activation time constant with an exponent of 1.0 and a maximum current of 100 pA. The inactivation rate for a single inactivation domain was assumed to be 10/s, with no recovery during the waveform. Time constants are those obtained for single exponential fits to the ensemble behavior, although multiple exponential components actually contribute to each trace. The predicted currents in the presence of 100 nM CTX are shown along the bottom, assuming the K_d values for CTX block shown across the top (K_{d1}, 2.0 nM; K_{d2}, 100 nM). Time constants show that the residual current in the presence of CTX decays more rapidly than the control BK_i current. The percentages of channels of each combination predicted from the binomial distribution for each average ratio of bk_s:bk_i subunits are listed at the bottom. (*B*) The simulated ensemble currents for the 3:1, 2:2, and 1:3 stoichiometries (*points with dotted lines*) shown in *A* are replotted along with the single exponential fits (*thin lines*) to the decay phase of the currents. The vertical line indicates the first fitted point. Although each simulated current contains multiple exponential components, as defined by the stoichiometries shown along the bottom in *A*, a single-exponential function provides a reasonable fit to the decay time course in each case. Time constants are given in *A*.

2. an inactivation-null, CTX-sensitive bk_s subunit

We assume that BK channels are tetramers (Shen et al., 1994), analogous to voltage-dependent K^+ channels (MacKinnon, 1991). CTX-resistant bk_i subunits are not insensitive to CTX, but exhibit a reduced sensitivity relative to bk_s subunits. Random assembly of subunits results in one BK_s single-channel phenotype and four BK_i phenotypes. Fig. 1 illustrates predicted average behavior both for a single channel comprising a particular ratio of bk_s:bk_i subunits and for a binomially distributed population of channels with a particular average ratio of bk_s:bk_i subunits. Predicted currents in the presence of 100 nM CTX are also shown along the bottom, given one assumption about CTX affinity, along with the predicted fraction of channels of particular stoichiometry. This model is a recapitulation of the experiment of MacKinnon et al. (1993), which defined the stoichiometry of *Shaker* K^+ channel inactivation. Functionally, this model is also essentially equivalent to one in which inactivation is conferred by differing numbers of an inactivation-competent accessory subunit that may associate specifically with a particular variant of core bk_s subunit.

This model predicts the following.

1. BK_i channels should contain multiple inactivation domains, but the average number of inactivation domains per channel may be less than four in many cases.

2. Cells with fewer inactivation domains per channel should have, on average, slower initial inactivation rates.

3. Cells with BK_i current should have variable CTX sensitivity, depending on the average number of bk_i subunits.

4. BK_i current in cells that are more resistant to CTX blockade should, on average, inactivate more rapidly.

5. During blockade by CTX, residual unblocked BK_i current should inactivate more rapidly than BK_i current before CTX application.

6. The frequency of occurrence of BK_s channels in patches with predominantly BK_i channels should be consistent with macrosopic estimates of the number of inactivation domains per channel.

All six of the above predictions are essentially independent, despite the fact that three pertain to the effect of CTX. Below, each of these predictions is evaluated experimentally. We caution that alternative models may account equally well for specific predictions, but that it is difficult to imagine alternative models that would account for the full set of predictions. We also caution that, although many of the properties of BK_i inactivation, including trypsin sensitivity and properties of recovery from inactivation, exhibit similarities to *Shaker*-type inactivation, the specific physical mechanism of block to permeation during the inactivation process remains unknown (e.g., Solaro et al., 1997).

It should be noted that, despite the fact that the heteromultimer model predicts that there should be up to four exponential components in the current inactivation time course, the decay process can generally be described by a single exponential time course that represents some weighted sum of all of the different components (e.g., MacKinnon et al., 1993). Even in the absence of stochastic noise or slow decay processes that have an impact on real experimental data, it would be difficult to discern the predicted four components, because they are not well separated in time, e.g., 25, 33, 50, and 100 ms. Even when the binomial distribution is dominated by only two components, those components will not be sufficiently well separated to allow careful estimation of their relative amplitude and time constants. Examples of the adequacy of single exponential fits to idealized currents based on stoichiometries of 3:1, 2:2, and 1:3, each predicted to have four exponential decay components, are shown in Fig. 1 *B*. Thus a single exponential adequately describes the hypothesized four component decays shown here and will have a predictable relationship to the stoichiometry of the channel population.

Inactivation of BK_i channels involves multiple, trypsin-sensitive, cytosolic domains

Inactivation of many voltage-dependent channels is trypsin-sensitive. The changes in current waveform during progressive trypsin digestion can provide information about the inactivation mechanism. For inactivation mechanisms involving a single trypsin-sensitive structure or the concerted action of multiple domains, all of which must be functional, all inactivating channels will inactivate with the same time course (e.g., Gonoi and Hille, 1987). In contrast, if inactivation results from multiple, largely independent domains, during trypsin digestion a progressive slowing in the time constant of inactivation (τ_i) is predicted, depending on the mean number of inactivation domains per channel within the population. For the simple case analogous to that examined for *Shaker*B K^+ channels (MacKinnon et al., 1993; Gomez-Lagunas and Armstrong, 1995), if normal channels inactivate because of the action of four independently acting inactivation domains and recovery from inactivation is slow, at most a fourfold slowing of τ_i would be expected as blocking domains were removed by trypsin.

BK_i channels in inside-out patches (1–10 channels) were activated by depolarizing voltage steps to +60 mV with 2 or 10 μM Ca^{2+}. In some cases a conditioning step to a negative potential (−120 or −140 mV) was used to remove partially resting inactivation (Fig. 2 *A*). Depending on the number of channels in the patch, 20–100 sweeps were used to generate each ensemble current. Trypsin (0.3 or 0.5 mg/ml) was then applied for 2–10 s to the cytosolic face of the patch. A second ensemble current was then generated, and this cycle was repeated through as many trypsin applications as was possible, or until inactivation was completely removed.

Brief trypsin applications result in a gradual slowing of the channel inactivation rate and a gradual increase in the number of channels that fail to inactivate at all (Fig. 2, *A* and *B*). The patch in Fig. 2 *A* contained two BK_i channels; τ_i for six separate current averages generated over ~20 min of recording before trypsin application was 29.4 ± 4.9 ms (mean ± SD of six ensemble averages). After the third 2-s application of trypsin, some slowing in τ_i of the ensemble average was observed. After trypsin, single sweeps show increased cases of bursts persisting later in the voltage step, even though all channels remain inactivating. For example, the second column of current traces in Fig. 2 *A* followed the sixth application of trypsin; the τ_i of the resulting ensemble current (Fig. 2 *B*) was 56 ms. After the 14th application of trypsin, one channel became noninactivating, whereas after the 16th application, both channels were totally noninactivating. In some cases, particularly with patches with fewer than five channels, during the progressive removal of inactivation produced by trypsin, although a single exponential could be fit to the current decay, two exponentials provided a better description of the inactivation time course.

Intrinsic lack of stationarity or stochastic fluctuations might complicate the interpretation of any trypsin-induced effects. Therefore, the stability of the BK_i inactivation rate was examined by repeated activation of single-channel currents over 30–40 min (Fig. 2 *C*). τ_i was determined from the average of currents activated by each sequential set of 20–30 voltage steps. For three patches shown in Fig. 2 *C*, there is some fluctuation in τ_i, presumably reflecting stochastic fluctuations in channel behavior. Despite these fluctuations, both τ_i (Fig. 2 *C*) and the ensemble current amplitude (not shown) are reasonably stable about the mean over this 30–40-min time period. In contrast, in those patches where trypsin was applied, trypsin rapidly and irreversibly results in a slowing of τ_i, which clearly falls outside the

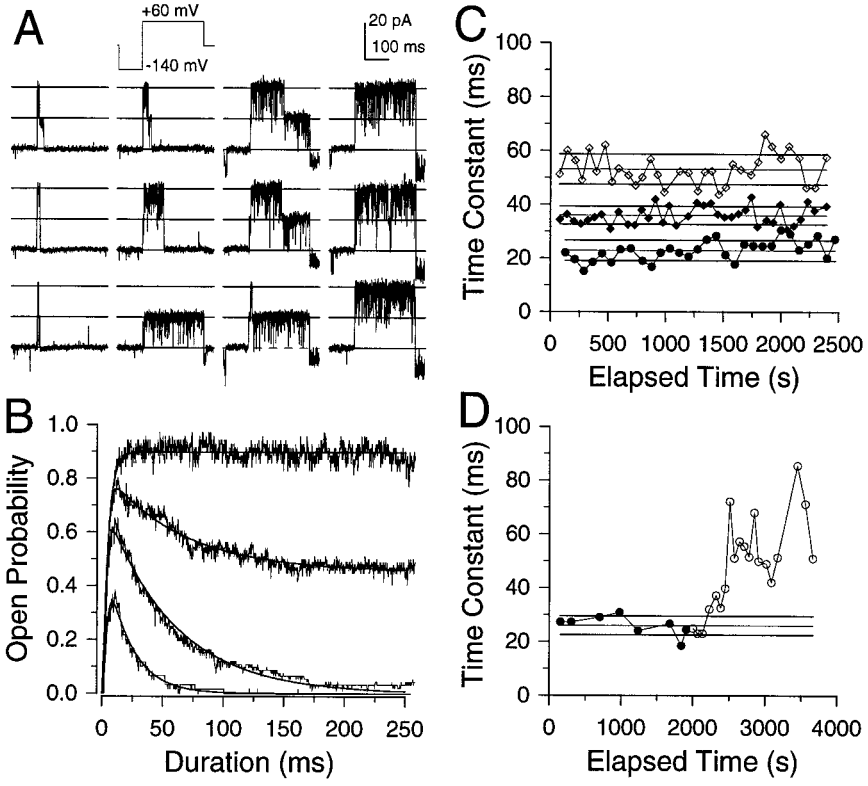

FIGURE 2 Slowing of the inactivation rate by trypsin suggests that BK_i inactivation involves multiple, cytosolic trypsin-sensitive inactivation domains. (*A*) Example sweeps from a patch with two BK_i channels are shown before and after the 6th, 14th, and 16th brief trypsin applications, respectively. The voltage protocol is indicated above the current traces. From a holding potential of −40, the patch was stepped to −140 mV for 100 ms before a 260-ms step to +60 mV. Three seconds separated the onset of each pulse sequence. After the 14th trypsin application, one channel becomes completely noninactivating, and after the 16th application, both channels become noninactivating. (*B*) The ensemble current averages, which included the traces in *A*, are plotted along with a fit of a Hodgkin-Huxley-type model to the activation and inactivation time course (Solaro et al., 1995). The inactivation time constants were 20.1 ms (30 sweeps), 56.0 ms (56 sweeps), and 62.8 ms (48 sweeps) for the inactivating currents. The noninactivating current was generated from 35 sweeps with a fitted maximum probability of being open of 0.89. Because the 100-ms step to −140 was insufficient to completely remove all resting inactivation, the change in peak ensemble current amplitude during the course of trypsin digestion largely reflects a trypsin-induced change in BK_i channel availability. Examination of all single sweeps for the four cases (control and 6th, 14th, and 16th trypsin applications) showed that the probability of opening was 0.53, 0.78, 0.91, and 1.0, respectively. The estimates for the first three cases would be in error by the fraction of sweeps in which both channels open sequentially but fail to overlap. This fraction is expected to be quite small, given mean burst durations of at least 20 ms and fast activation rates. (*C*) The stationarity of the inactivation time constant for BK_i channels is shown for three inside-out patches. Currents were activated with a protocol similar to that used in *A*. Ensemble current averages were generated from the idealized openings during the depolarizing step. Each point corresponds to the time constant of inactivation for an ensemble generated from ~20 voltage steps. These patches contained 7 BK_i (*bottom*), 15 BK_i (*middle*), and 15 BK_i with 1 BK_s channel (*top*). The thin, horizontal solid line in each case corresponds to the mean of all determinations for the given patch, and the thicker lines indicate the limits of the standard deviation. (*D*) The time course of removal of inactivation by trypsin is shown for a patch that contained 10 BK_i channels. Closed symbols correspond to time constants of inactivation before trypsin application, and open symbols correspond to time constants after trypsin application. The mean and standard deviation of estimates before trypsin application are indicated by the horizontal lines, as in *A*.

range of variability observed before the onset of trypsin action (Fig. 2 *D*).

Slowing of τ_i was observed in 15 of 15 patches in which some removal of inactivation was observed. In patches in which almost complete removal of inactivation was achieved, prolongations exhibited considerable variability, ranging from 1.6-fold to a little over 4-fold. Qualitatively, the simplest interpretation of the slowing of inactivation by trypsin is that, like voltage-dependent K^+ channels but unlike voltage-dependent Na^+ channels, inactivation of BK_i channels results from multiple (perhaps up to four) independent cytosolic domains. However, in contrast to voltage-dependent K^+ channel inactivation, the results suggest that there may be some variability in the average number of inactivation domains per channel in a population. We remain cautious about the interpretation of the magnitude of the slowing of τ_i, because the slower time constants were difficult to fit, thus compromising estimates of the limiting τ_i. We therefore turned to the use of peptidase removal of inactivation in whole-cell recordings to address this issue in more detail.

Peptidase removal of inactivation in whole-cell recordings argues for fewer than four inactivation domains per channel

Because whole-cell recordings reflect the behavior of perhaps 100–500 BK channels, we assume that trypsin-in-

duced alterations in macroscopic current should better follow expectations based on a changing, but binomial, distribution of inactivation domains among channels, than would channels in excised patch experiments. Experiments described in Fig. 3 establish the utility of the method. Cells were voltage-clamped with pipettes containing 10 μM Ca^{2+}. Voltage steps to +60 mV result in a robust activation of an inactivating outward current, which is strictly dependent on cytosolic Ca^{2+} (Solaro et al., 1995). This BK_i current was relatively stable, in terms of τ_i (Fig. 3, *B* and *C*) and amplitude (Fig. 3 *D*), for over 15 min of recording. Because these whole-cell currents also contain some noninactivating voltage-dependent K^+ current, it is not possible to determine how much of the sustained current reflects BK current, although in the absence of cytosolic Ca^{2+} sustained voltage-dependent K^+ current is typically less than 1 nA (Fig. 3 *E*; also Prakriya et al., 1996). In the presence of 1 mM external 4-AP, we have never observed inactivating current with 0 pipette Ca^{2+}. Because experiments described below examined the effects of cytosolic peptidase on BK_i inactivation, the effect of trypsin on whole-cell voltage-dependent outward current was also examined in the absence of pipette Ca^{2+}. The lack of effect of trypsin on voltage-dependent outward current is shown in Fig. 3, *E* and *F*. Trypsin does not unmask any noninactivating voltage-dependent K^+ current that might complicate the interpretation of results described below.

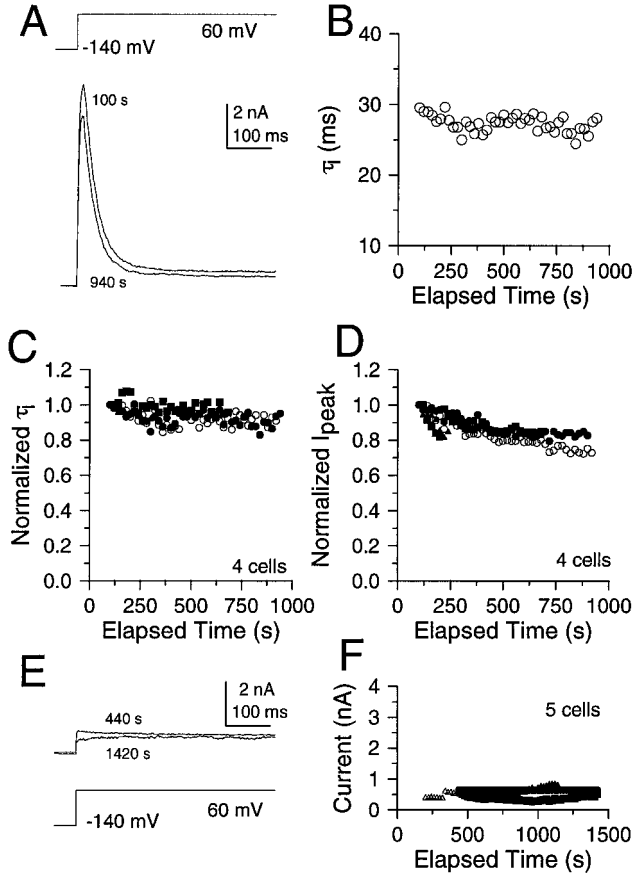

FIGURE 3 BK current can be reliably elicited in whole-cell recordings with defined pipette Ca^{2+}. (*A*) Currents elicited at +60 mV after a 200-ms step to −140 mV with 10 μM pipette [Ca^{2+}] are shown at 100 and 940 s after breaking into the cell. The holding potential was −60 mV. Virtually all current used in this procedure is BK current (Solaro et al., 1995). The extracellular saline contained 1 mM 4-AP. In the absence of pipette Ca^{2+}, no inactivating current is elicited in these cells. (*B*) Stability of τ_i measured over 16 min for the cell in *A*. (*C* and *D*) Plots of the stability of τ_i (*C*) and peak current (*D*) for four different cells. (*E*) Whole-cell current was elicited as in *A*, but with a pipette containing 0.5 mg/ml trypsin with 0 extracellular Ca^{2+}. (*F*) Peak current amplitude for four separate cells in which the pipette contained trypsin, but 0 Ca^{2+}, is plotted as a function of recording time.

As exploited in a study of mixtures of inactivating and noninactivating *Shaker*B K^+ channel subunits (MacKinnon et al., 1993), for a population of channels with a particular average number of inactivation domains per channel, τ_i should display a predictable relationship to the fraction of channels that are completely noninactivating. Here we have taken a similar approach, using enzyme-mediated digestion of inactivation to examine the relationship between τ_i and the fraction of maximum BK current (BK_{max}) that is noninactivating current (f_{ss}). In Fig. 4, we show several types of predictions. First, the relationship between τ_i and f_{ss} is defined, given the assumption that each channel has a maximum of *N* inactivation domains and that each channel starts with *N* inactivation domains (Fig. 4 *A*). As digestion occurs, the number of inactivation domains per channel is assumed to follow a binomial distribution. This is identical to the case examined for *Shaker*B K^+ channels (MacKinnon et al., 1993). Second, the relationship between τ_i and f_{ss} is provided, given the assumption that each channel can have a maximum of four inactivation domains, but the channel stoichiometries are binomially distributed around some value less than 4 before the onset of enzyme digestion (Fig. 4 *B*). In such a case, there will be some number of channels with no inactivation domains that would produce a steady-state BK current before the onset of the action of trypsin. Because experimentally we are unable to determine the resting amount of noninactivating BK current (e.g., Figs. 5 and 6), the predictions shown here calculate the change in apparent f_{ss}, ignoring the initial small steady-state current expected in all cases with an average number of inactivation domains of two or more. Third, the relationship between τ_i and f_{ss} is given for situations in which all channels have four inactivation domains, but there are either positive or negative interactions that affect the rate of inactivation (Fig. 4 *C*). Negative interactions between inactivation domains slow the rate at which any individual inactivation domain may reach a blocking position. Positive interactions might arise, for example, if adjacent domains, by reducing the effective degrees of freedom available to a given subunit, increase the likelihood that a given domain can move to a blocking position. It should be noted that, if there is steric hindrance between inactivation domains (Fig. 4 *C*), a prolongation of less than fourfold may result, even with four inactivation domains. Finally, we consider the case in which there is an additional slow component of inactivation that becomes revealed as fast inactivation is removed (Fig. 4 *D*).

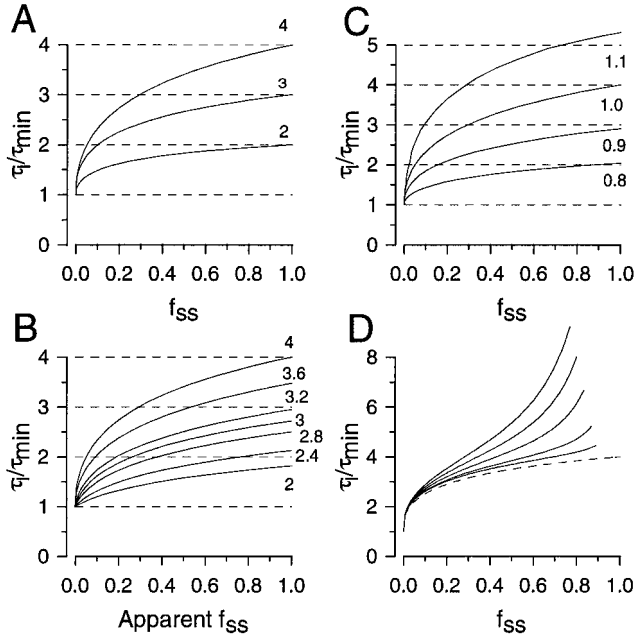

FIGURE 4 Predictions for the relationship between prolongation of τ_i versus f_{ss} during the action of trypsin. For all cases, currents were simulated as decribed in Materials and Methods, assuming a Hodgkin-Huxley activation scheme with five channel stoichiometries. Simulated currents were then fit to obtain a single time constant of inactivation and a value for the steady-state current. From these, the prolongation in τ_i and the change in f_{ss} were determined. (*A*) Standard predictions for the relationship between τ_i and f_{ss} are given for the case where the population of channels is initially homogeneous, all beginning with either four, three, or two inactivation domains per channel. This is identical to the case considered by MacKinnon (1991). (*B*) The channel population begins with a binomially distributed population with some particular fraction of bk_i subunits (*numbers on the right*). Thus, in this case, f_{ss} represents an apparent f_{ss} in which the initial steady-state current level is set to 0. For 50% bk_i subunits, there will be a steady-state current of ~6.25% of the peak current. The thickened lines correspond to the standard predictions shown in *A*, with all channels beginning with either three or two inactivation domains. (*C*) Consequences of the lack of independence among inactivation domains. Currents were simulated as above, with the addition that the inactivation rate depended on the number of inactivation domains. The inactivation rate of any inactivation domain was either increased or reduced by some factor dependent on the number of other inactivation domains in the channel. Thus, if the intrinsic rate of inactivation of one ball is k_f, then τ_i for channels containing N inactivation domains is given by $\tau = 1/(N*x^{N-1}*k_f)$ where x is the fraction by which the inactivation rate is affected by each additional inactivation domain. (*D*) f_{ss} and τ_i were calculated based an inactivation model in which, in addition to fast inactivation involving one to four inactivation domains, there was a slow inactivation process unaffected by trypsin. Amplitudes and time constants were calculated based on

$$I_s \underset{k_{sr}}{\overset{k_s}{\rightleftharpoons}} O \underset{k_{fr}}{\overset{m*k_f}{\rightleftharpoons}} I_f$$

where the rate of fast inactivation (m * k_f) for a particular channel stoichiometry was determined by m (the number of inactivation domains), and the rate of recovery from fast inactivation, k_{fr}, was set to 0. For all curves, k_s = 1/s and k_f = 10/s. k_{sr} varied from 3.3/s to 8/s. Note that even at early times in the digestion process, a slow inactivation process will result in a prolongation of τ_i, suggestive of $m > 4$.

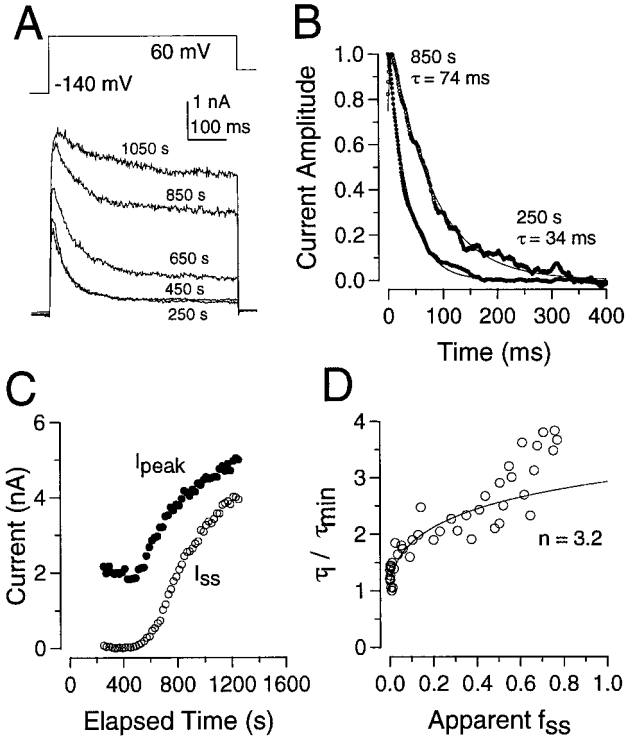

FIGURE 5 The slowing of inactivation by trypsin suggests that BK_i channels have, on average, fewer than four inactivation domains. (*A*) Outward currents were elicited every 20 s by the indicated voltage protocol. The cell was held at −60 mV before the 100-ms step to −140 mV. The experimental conditions were identical to those described in Fig. 3, except that the recording pipette contained 0.5 mg/ml trypsin. Each trace shows primarily BK current at different times after initiation of whole-cell recording. Trypsin gradually slows inactivation. (*B*) The current decay time courses at two time points (250 and 850 s) are fit to a single exponential. (*C*) The changes in peak and noninactivating current during the digestion process are shown. (*D*) The relationship between prolongation of τ_i and the fractional noninactivating current as a function of peak current is plotted. Peak current was defined from the maximum current elicited during the trypsin digestion process. The solid curve is the prediction based on the assumption that, at $t = 0$, channels contained an average of 3.2 trypsin-sensitive inactivation domains binomially distributed within the channel population.

The consequence of such an additional, trypsin-resistant inactivation process is to increase the initial apparent change in τ_i as a function of f_{ss}, while resulting in a limiting asymptote of f_{ss}.

Cells were studied with whole-cell recording procedures in which trypsin or papain was backfilled into the recording pipette. After seal formation, enzyme was allowed to equilibrate into the pipette tip before initiation of whole-cell recording (see Materials and Methods). With this procedure, upon initiation of whole-cell recording, the delay until the onset of removal of inactivation was substantially reduced. Results for one cell are shown in Fig. 5. Currents activated by voltage steps to +60 mV at the indicated times after initiation of whole-cell recording are displayed (Fig. 5 *A*), along with examples of the decay time course at two time points after the introduction of trypsin (Fig. 5 *B*). Both the amplitude of peak outward current and the residual nonin-

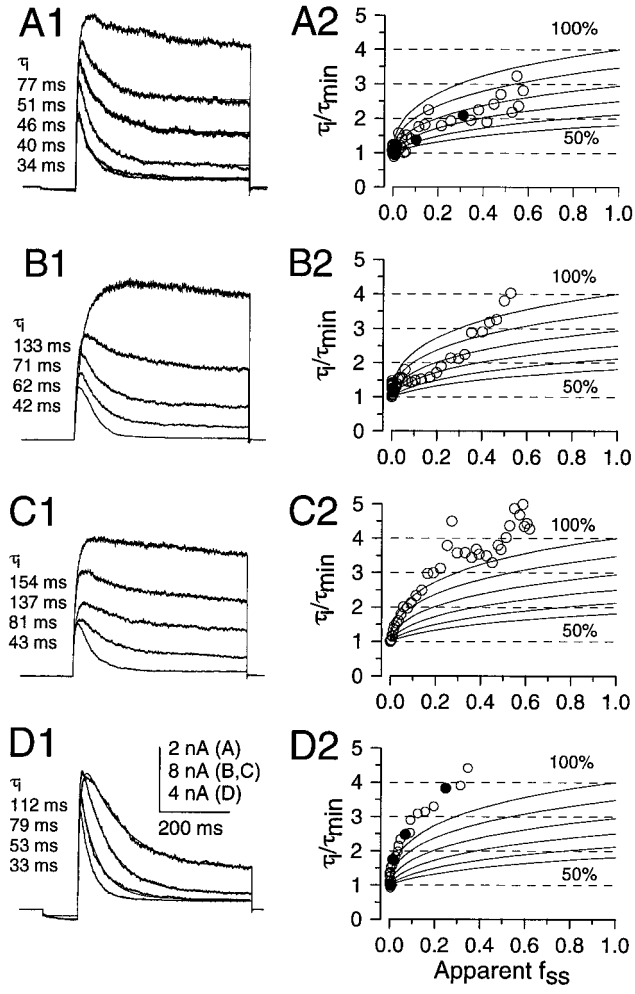

FIGURE 6 Changes in BK_i current during digestion by trypsin. *A–D* correspond to four different cells in which trypsin was used to remove BK_i inactivation. The voltage protocol was as in Fig. 5, except that in *B* and *C* a 200-ms step to −140 mV preceded the step to +60 mV. In *A1–D1*, example traces of BK_i current at different times during the digestion process are shown, along with measured time constants of inactivation. Cells are shown in order of smaller to large changes in τ_i during the initial stages of trypsin digestion. In *A2–D2*, the change in τ_i is plotted as a function of f_{ss} for each cell. For cells in *A–C*, BK_{max} was determined from the largest BK current amplitude late in the digestion process. For the cell in *D*, the BK_{max} was taken from the largest current in the set of traces. Because complete digestion was not achieved, values of f_{ss} in this case are overestimates. The solid curves in *A2–D2* come from the predictions shown in Fig. 3 *B*, for assumptions of two to four inactivation domains per channel (mole fractions of bk_i subunits of 0.5, 0.6, 0.7, 0.8, 0.9, and 1.0). The pipette saline used for these experiments included 35 mM Cs^+ to minimize total BK current. C_m and R_s for each cell, respectively, were 5.0 pF and 2.2 MΩ, 8.6 pF and 5.0 MΩ, 11.4 pF and 4.4 MΩ, and 7.8 pF and 4.0 MΩ for *A–D*, respectively. R_s compensation was at least 80% in each case.

activating current increase during the trypsin digestion process (Fig. 5 *C*). A large portion of the increase in peak current is likely to result from a change in the amount of residual inactivation persisting at the time of the voltage step to +60 mV, as suggested in Fig. 2 *A*. From the peak current measured at the end of the trypsin digestion process and the residual noninactivating current at each point in time, f_{ss} was determined. The amount of prolongation of τ_i is plotted as a function of f_{ss}, along with the predicted relationship for a population of channels beginning with an average number of inactivation domains of 3 (Fig. 5 *D*). The slowing of the inactivation process by trypsin supports the view that inactivation of BK_i channels involves multiple, inactivation domains. Furthermore, the change in τ_i as a function of residual noninactivating current suggests that inactivation involves fewer than four inactivation domains.

Considerable variability was observed in the relationship between the changes in τ_i and the changes in apparent f_{ss}. Examples of changes in current waveform during the action of trypsin are shown for four cells in Fig. 6, *A–D*, along with the measured changes in τ_i and f_{ss}. One key feature of the results can be inferred simply by inspection of the current traces. Specifically, there is substantial variability in the amount of change in τ_i with even small changes in steady-state current. For example, with changes in steady-state current that correspond to less than 20% of the initial peak current, the changes in τ_i illustrated in Fig. 6 range from 1.3 to 2.4. For a population of cells with a homogeneous set of channels among all cells, we could expect that, given a particular fractional increase in steady-state current, there should be a particular increase in τ_i. Qualitatively, the changes seen in the current traces appear contradictory to this expectation.

The right-hand panels of Fig. 6 plot the observed changes in τ_i versus the apparent f_{ss} for four cells. Although complete removal of inactivation was not obtained for the cell shown in Fig. 6 *D*, this cell was included to illustrate the large changes in τ_i that were observed, in this case, with only small changes in steady-state current. The values for f_{ss} were determined based on the peak of the largest recorded current. We expect this value to be an underestimate, and thus the apparent f_{ss} values would be even smaller than calculated in this case. The primary point of these plots is that there is substantial variability in the magnitude of the changes in τ_i with changes in apparent f_{ss}. When the experimental points are compared to the theoretical relationship between changes in τ_i and apparent f_{ss}, the results are consistent with the hypothesis that BK channels in chromaffin cells may exhibit substantial variability in the average number of inactivation domains per channel.

A number of factors may complicate the reliability of the estimates of the number of inactivation domains acquired in the above experiments. The most precarious parameter in defining the relationship between changes in τ_i and f_{ss} is the measurement of the maximum amount of BK current or BK_{max}. In stable cells, BK_{max} can presumably be determined directly from the peak current at the end of the trypsin digestion period, as shown for the cells in Fig. 6, *A–C*. For each of the cases illustrated, the initial transient BK current is a similar fraction of the final peak BK current observed after the removal of inactivation. Furthermore, this increase in current amplitude is similar to that observed in Fig. 2 *A* from an excised inside-out patch studied with a

similar voltage protocol with identical submembrane $[Ca^{2+}]$. This consistency suggests that such direct measurements of BK_{max} are probably fairly reliable. If this method were substantially underestimating the true peak BK current, this would shift f_{ss} values leftward for a given prolongation in τ_i. Assuming that BK_{max} was underestimated by 50%, a corrected f_{ss} would be shifted 33%. Although it unlikely that our estimates of peak BK current are in error by this amount, this amount of shift would be insufficient to account for the estimated values of less than 4 for the number of inactivation domains per channel.

Two other considerations were also used to ensure our confidence in any particular estimate. First, results from a cell were considered more reliable if the peak current amplitude exhibited a continuous, monotonic increase during the trypsin digestion process. In some cells, transient reduction of the access resistance could result in anomalous decrements in the peak current increase, which would also be associated with anomalous changes in τ_i, presumably as a result of changes in the cytosolic $[Ca^{2+}]$. Second, cells in which there was little or no detectable change in current resulting from the step to −140 mV during the trypsin digestion process were considered more reliable. The example shown in Fig. 6 *D* in which large changes in τ_i were observed fails to meet either of these two criteria, but this cell has been included for illustrative purposes because, of all cells studied, it comes closest to the behavior expected for a population of channels containing four inactivation domains per channel.

To summarize these experiments, trypsin produced a slowing of inactivation in all 21 of the cells examined. On average, τ_i was prolonged by about two- to threefold by the action of trypsin (or papain). Furthermore, the initial change in τ_i versus f_{ss} followed a relationship consistent with an initial average of about two to three inactivation domains per channel. At late times during the action of trypsin, there was a slow component of inactivation, which in some cases even exceeded four times the original τ_i. Unexpectedly slow components of inactivation have been observed during both papain-induced removal of *Shaker* inactivation (Gomez-Lagunas and Armstrong, 1995) and papain-induced removal of Na^+ current inactivation (Gonoi and Hille, 1987). As shown in Fig. 4 *D*, a second, slower, independent inactivation process unaffected by trypsin can result in upward curvature in the relationship between f_{ss} and prolongation of τ_i. Although this residual inactivation may arise from other intrinsic inactivation processes, from exogenous blocking molecules, or from trypsin-released blocking particles, we have no information that would allow us to discern among these possibilities. In any case, it is clear that caution must be used in interpreting τ_i values at late digestion times. Because at longer times of digestion trypsin may begin to exert other effects on BK channel function, the shorter periods of enzyme action are likely to be more reliable. Fortunately, the largest predicted changes in τ_i are expected over changes in f_{ss} of up to 0.5. Because this region of greatest predictive power is associated with the shorter periods of trypsin application, we consider the shape of the relationship between τ_i/τ_{min} versus f_{ss} during the initial stages of digestion (i.e., f_{ss} values up to ~0.4–0.5) to be the most useful predictor of the initial number of inactivation domains. The assumption of two to three inactivation domains per channel appears to best account for the cells illustrated in Fig. 5 and Fig. 6, *A–C*.

The change in fraction of noninactivating current as a function of digestion time was also used to provide an independent estimate of the number of inactivation domains per channel (Gomez-Lagunas and Armstrong, 1995), in conjunction with the predicted time course of increase in the enzyme concentration in the cell (based on the pipette access resistance; Pusch and Neher, 1988). Similar to the results with *Shaker*B channels (Gomez-Lagunas and Armstrong, 1995), the shape of the curve of I_{ss}/I_{peak} as a function of time deviated from all simple predictions. However, in contrast to the results from *Shaker* channels in which channels were expected to start with a defined stoichiometry of four inactivation domains per channel, the observed changes qualitatively fell in a range of values that were more consistent with an average of perhaps two to three (results not shown) inactivation domains per channel.

Changes in current waveform during trypsin digestion are consistent with a heteromultimeric model

The above results provide initial qualitative support for the idea that BK_i channels in chromaffin cells may contain zero to four inactivation domains and that the average number of such inactivation domains per channel is generally less than four. To provide an additional test of this idea, we tested whether the heteromultimeric model could account for the changes in current waveform during the peptidase digestion process by evaluating two distinct cases. In one case, we assumed that the initial inactivation rate reflected a homomultimeric population of channels, each containing four inactivation domains, and in the second case we assumed that the population of channels was heteromultimeric, with less than a full complement of inactivation domains per channel.

To describe the current waveform at any point in time, we used a Hodgkin-Huxley activation model as described in Materials and Methods. We used this model to fit 52 current waveforms obtained every 20 s over ~900 s of recording. Trypsin-induced changes in current waveform were first observed after ~180 s. Given that removal of inactivation results in changes in the amount of resting inactivation after 100-ms or 200-ms periods at −140 mV (e.g., Fig. 2 *A*), the changes in peak current amplitude during the removal of inactivation are not entirely predictable in the absence of a complete model of inactivation. However, the changes in observed time course and amount of residual noninactivating current are still of use in evaluation of the proposed heteromultimer model.

The steady-state level of current in these macroscopic recordings (Fig. 6) is determined by two factors: current

arising from sources other than BK channels (which we call I_{KV}) and the amount of BK current that is noninactivating. In accordance with the model, the noninactivating BK current is defined by the mole fraction of bk_i subunits in the cell. If we knew explicitly how much of the steady-state current was BK current, this would define explicitly the mole fraction of bk_i subunits. However, experimentally, there is no convenient way of independently identifying the amount of steady-state current arising from BK channels (however, see Fig. 14). Therefore, for this analysis we examined two cases, each with a different assumption that constrains the amount of steady-state current that must be BK current. In the first case, we assume that, before the action of trypsin, all channels in a chromaffin cell contain a full complement of four inactivation domains. With this assumption, all steady-state current before the removal of inactivation by trypsin arises from I_{KV}. In the second case, we assume that the minimum τ_i is ~25 ms. This value constrains the fraction of BK current that is noninactivating and, therefore, defines the contaminating I_{KV} before the onset of trypsin digestion.

For the first case, using the initial set of current waveforms before the onset of digestion and assuming that the percentage of bk_i subunits is 100, estimates of I_{KV} and the minimum time constant (τ_{min}) resulting from channels with four inactivation domains were defined. For the cell shown in Fig. 7 *A*, the resulting τ_{min} was 39 ms with ~220 pA of contaminating current. We then assumed that these parameters are unaffected by the action of trypsin, allowing us to constrain these values in subsequent fits to currents obtained after the trypsin digestion process has begun. With these values, fits to the current waveforms at different times in the digestion process failed to adequately account for the changes in shape in the current waveforms (Fig. 7 *A*). The

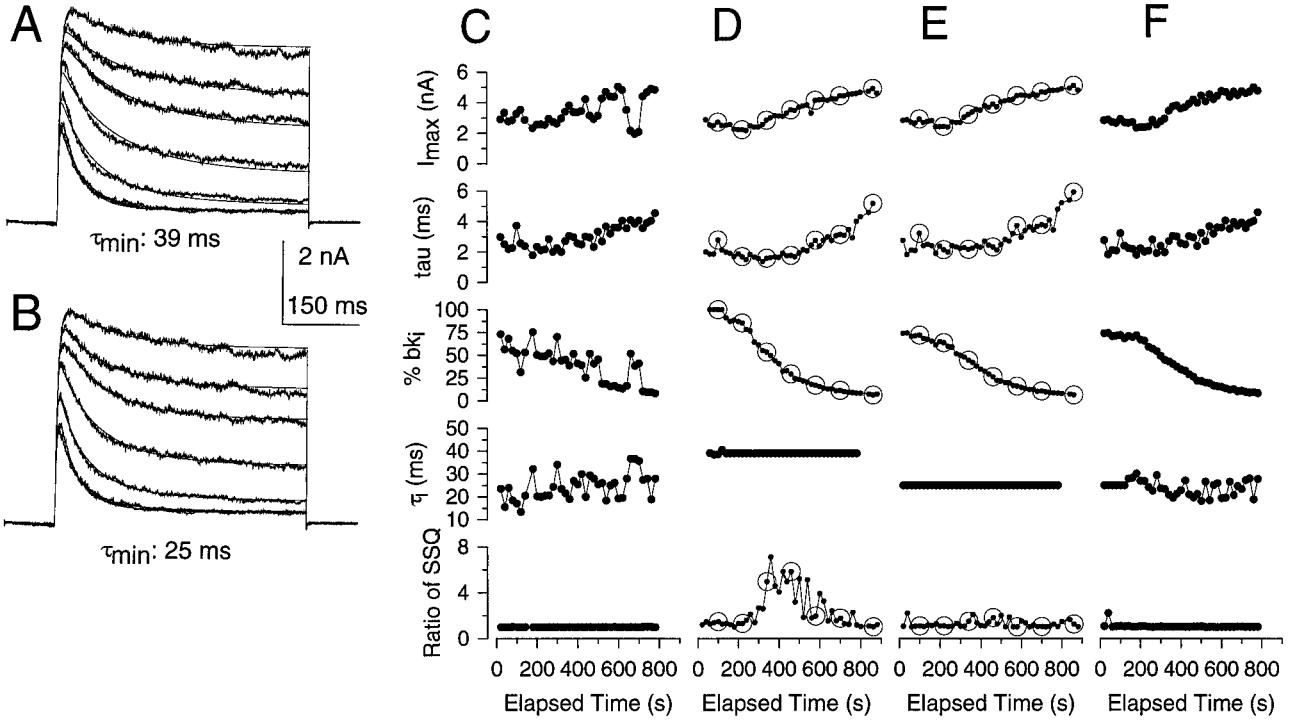

FIGURE 7 Changes in current waveform during trypsin digestion are consistent with a heteromultimer model. A chromaffin cell was held at −60 mV and, every 20 s, was stepped to −140 mV for 100 ms before a 500-ms step to +60 mV. The pipette saline contained 10 μM Ca^{2+} and was backfilled with trypsin. Traces are the 6th, 12th, 18th, 24th, 30th, 36th, and 43rd after onset of whole-cell recording. (*A*) Traces 4–7 were fit with a Hodgkin-Huxley model, as described in Materials and Methods, in which the percentage of bk_i subunits in the cell was constrained to 100%. This defined τ_{min} as 39 ms, with 220 pA of contaminating voltage-dependent outward current. For subsequent fits of the currents, τ_{min} was then constrained to 39 ms and I_{KV} to 220 pA. Note the poor fit resulting from this assumption for traces obtained during partial digestion. (*B*) For sweeps 4–7, τ_{min} was constrained to 25 ms, based on other estimates of τ_{min} described below. This resulted in an estimate of I_{KV} of 188 pA, with an initial percentage of bk_i subunits of 74%. Constraining t_{min} to 25 ms and I_{KV} to 188 pA for all subsequent traces resulted in the best fits shown by the solid lines. (*C–F*) Values for the peak current amplitude (I_{max}), activation time constant (τ_a), and percentage bk_i subunits are plotted for four fitting procedures. In *C*, all parameters were unconstrained. Because some parameters are strongly dependent on others (e.g., I_{KV} and % bk_i subunits), the values are not well determined, but the best fit provides a measure of the optimal sum of squares (SSQ) for the generalized model. The bottom panel in each column therefore plots the SSQ of a fit divided by the SSQ obtained with all parameters unconstrained (ratio of SSQ). An SSQ ratio near 1 implies that the constraints of a particular set of assumptions result in a reasonable fit to the currents. In *D*, fits were generated as described in *A*, with open circles indicative of traces shown in *A*. At intermediate times during the digestion process, the ratio of SSQ deviated considerably from 1. In *E*, fits were generated as described in *B*, with open circles indicative of traces shown in *B*. Despite the fact that two parameters were constrained over all sweeps, the resulting ratio of SSQ was quite stable, being near 1 over the entire digestion time course. In *F*, the fit procedure was similar to that in *E*, except that τ_{min} was unconstrained, and I_{KV} was 188 pA. With this procedure, all τ_{min} values providing the best fit were between 18 and 30 ms, consistent with the idea that τ_{min} is ~25 ms.

changes in peak current, current activation time constant, percentage of bk_i subunits, and τ_i are plotted in Fig. 7 *D* and compared to parameter values derived from other assumptions (Fig. 7, *C*, *E*, *F*). As a measure of the adequacy of the fits, a normalized measure of the sum of squares (SSQ) of the fit is plotted in the bottom row of Fig. 7 *D*. To obtain this measure, the raw currents were fit by the model with all parameters unconstrained (Fig. 7 *C*). Although correlations among parameters meant that no parameters are sharply defined in this case, the fit with unconstrained parameters provides an optimal estimate of the SSQ that can be used for evaluation of fits obtained with other assumptions. Thus, for each fitting procedure, the resulting SSQ was normalized to that obtained with all parameters unconstrained (Fig. 7, *C–F*, *bottom row*). The deviation from one of the ratios of the SSQ seen in Fig. 7 *D* provides a qualitative indication of the failure of the homomultimer model to account for the changes in time course during the trypsin digestion process. Clearly, the assumption that all channels initially contain four inactivation domains results in changes in current waveform that are inconsistent with the expectations of this assumption.

The results of fitting the same set of current waveforms with the second set of assumptions is shown in Fig. 7 *B*. Based on other results that suggest that the limiting τ_{min} for channels containing four inactivation domains is ~20–30 ms, we constrained τ_{min} to 25 ms. From sweeps 4 through 7, this results in an estimate of the initial contaminating I_{KV} of 188 pA. Making the same assumption as above, i.e., that τ_{min} and the contaminating current will be unaffected by the action of trypsin, we then constrained these values during subsequent fits of all other traces. These assumptions result in rather reasonable approximations of the actual data traces over the entire time course of trypsin digestion (Fig. 7 *B*). The resulting values and normalized SSQ are plotted in Fig. 7 *E*. For comparison, Fig. 7 *F* shows resulting values from a fit in which I_{KV}, but no other parameter, was constrained to 188 pA. In this case, all resulting estimates of τ_{min} cluster around 25 ms, providing additional support for the idea that, in a cell with an initial inactivation time constant of ~39 ms, current waveforms are best accounted for by a model in which channels are heteromultimers with a limiting τ_{min} of ~25 ms.

Given the success of the heteromultimer model in accounting for the current waveform at all times in the digestion process, this analysis suggests that in this cell BK_i channels initially contained, on average, about three inactivation domains per channel, decreasing to ~0.06 inactivation domains per channel. Furthermore, the changes in the peak current amplitude seen during the trypsin digestion process are qualitatively consistent with those expected for the amount of removal of resting inactivation observed in Fig. 2. Finally, at later times in the digestion process, there is some change in τ_a, the rate of current activation, consistent with earlier observations that trypsin may have some effect on BK current activation rates (Solaro et al., 1995; Lingle et al., 1996).

This analysis allows the following conclusion. Not only does the slowing of inactivation by trypsin suggest that BK_i channels contain multiple inactivation domains, but, if the maximum number of inactivation domains is four, the changes in current waveform can only be well described by a model in which channels contain, on average, fewer than four inactivation domains. This analysis does not consider homomultimer models in which the maximum number of inactivation domains per channels is something other than four. However, the observation that the number of inactivation domains per channel exhibits substantial variability among cells argues against a simple homomultimer model involving something other than four inactivation domains.

Larger estimates of the average number of inactivation domains correlate with faster initial τ_i

Using the relationship between changes in τ_i and f_{ss}, we determined that values for the number of inactivation domains per channel ranged from ~1.7 up to ~4 for a set of 22 cells, with a mean value of 2.9 ± 0.4. The extent to which the trypsin-induced prolongation of τ_i shows less than a fourfold increase is consistent with the idea that the average number of inactivation domains is less than four in most cells. If this were the case, we would also expect there to be a correlation between the estimate of average number of inactivation domains per channel with the initial τ_i in a cell. Cells with faster initial inactivation rates would be expected, on average, to have a higher average number of inactivation domains per channel. This relationship is plotted in Fig. 8. Although there is considerable scatter, there is

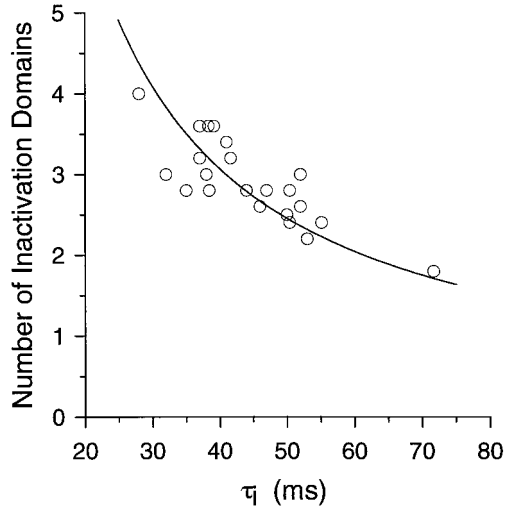

FIGURE 8 Cells with a larger estimated average number of inactivation domains per channel tend to inactivate more rapidly. The average number of inactivation domains per channel estimated from the relationship shown in Fig. 5 is plotted against the initial τ_i for each cell. More slowly inactivating cells have a smaller estimated average number of inactivation domains per channel. The solid line has no theoretical significance, but suggests that, with four inactivation domains per channel, the limiting $\tau_i \approx$ 25–30 ms.

a strong tendency for slower initial inactivation rates to be associated with a smaller estimate of average number of inactivation domains. Assuming that any cell can have at most an average of four inactivation domains per channel, the limiting τ_i appears to approach ~25 ms. As noted above, a less than fourfold slowing during the action of trypsin might also result from lack of independence among inactivation domains during the inactivation process. However, in such a case, we would not expect there to be a correlation between faster τ_i with a larger average number of inactivation domains per channel. Similarly, the variability in the fractional prolongation of τ_i produced by trypsin would seem to be more consistent with true variability in the number of inactivation domains rather than the result of a lack of independence in the inactivation process.

Removal of inactivation by trypsin does not affect rates of recovery from inactivation

Examination of the time course of recovery from inactivation may also be informative about the number and independence of inactivation domains. To address this issue, the effect of trypsin on the time course of recovery from inactivation was examined in inside-out patches bathed with 10 μM Ca^{2+}. Current averages were generated from BK channel openings activated with a sequence of paired pulses (Fig. 9 *A*) with interpulse recovery intervals at −140 mV from 1.5 to 800 ms. Trypsin was briefly applied, and then the recovery protocol was repeated. Both the inactivation time course (Fig. 9 *B*) and the fractional recovery as a function of recovery time were determined (Fig. 9 *C*). At [Ca^{2+}] from 4 to 60 μM, recovery at potentials from −40 to −100 mV is described by two exponential components (Ding et al., 1996). However, at −140 mV and 10 μM, recovery can be adequately described by a single exponential function with a time constant of 16.3 ± 5.1 ms (mean ± SD; $n = 7$). For *Shaker* inactivation (MacKinnon et al., 1993), irrespective of the number of inactivation domains, once inactivation has occurred, recovery is thought to be controlled solely by the rate of dissociation of a single inactivation domain. On the other hand, if a single domain is necessary to produce inactivation, but multiple domains can move into independent positions, each sufficient to maintain inactivation, recovery from inactivation would be expected to exhibit a dependence on the number of residual trypsin-sensitive domains.

For the patch shown in Fig. 9, irrespective of the trypsin-induced slowing of the inactivation rate (Fig. 9 *B*), no change in the recovery time constant (τ_r) was observed (Fig. 9 *C*). Thus, whatever the trypsin-induced alteration in channel structure that results in a prolongation of τ_i, neither an increase nor a decrease in τ_r is observed. In four cells from a set of seven, there was no significant change in τ_r as inactivation was removed. In the other three, there was an immediate increase in recovery rate after the first trypsin application. However, subsequent trypsin applications produced no additional change in recovery, although the rate of inactivation continued to slow with trypsin in these three cells. Thus the rapid, trypsin-induced change in recovery in some cells does not have the features expected for gradual digestion of inactivation domains. We therefore conclude that gradual removal of inactivation by trypsin is not associated with a change in the rate of recovery from inactivation.

We have evaluated the expected time course of recovery for a mechanism in which each of N inactivation domains must independently dissociate to produce recovery. Such a mechanism is functionally comparable to a Hodgkin-Huxley gating scheme in which two to four particles must each undergo some transition before channels are recovered from inactivation. For such a mechanism, recovery will exhibit an appreciable lag. The best fit predictions for recovery involving two or four inactivation particles are displayed over the data in Fig. 9 *C*. The actual recovery from inactivation proceeds in a fashion most consistent with the involvement of a single inactivation domain/particle. In Fig. 9 *D*, data points before trypsin and after the second trypsin application are plotted. The solid line provides the fitted recovery time course, assuming that the population of channels start with an average of 2.5 particles per channel, all of which participate in the recovery process. The dotted line provides the expected shift in the recovery time course, if the only effect of trypsin is to change the average number of inactivation particles per channel from 2.5 to 1. This shows that a trypsin-induced change in the number of inactivation particles participating in the recovery process would result in both a shift in apparent recovery time course and a change in apparent sigmoidicity. Such a change in sigmoidicity is not observed (Fig. 9 *E*).

This analysis suggests that changes in apparent sigmoidicity in the recovery process may perhaps be the strongest diagnostic parameter for assessing whether multiple particles may independently participate in a recovery process (see also Kuo and Bean, 1994). The single inactivation particle model predicts that neither recovery rate nor sigmoidicity will change as trypsin removes inactivation domains, as is observed. We conclude that the lack of sigmoidicity in the recovery process and lack of effect of trypsin on that recovery process argue that only a single inactivation particle must dissociate to remove inactivation.

BK_i current in chromaffin cells is relatively resistant to blockade by CTX

The CTX sensitivity of whole-cell BK current was examined in two types of experiments. In one set of experiments, Ca^{2+} influx was used to activate BK current during perforated-patch recordings (Horn and Marty, 1988). In the second set of experiments, depolarizing voltage steps with 10 μM pipette Ca^{2+} were used to activate BK current. The former method offered the advantage that the Ca^{2+}-dependent component of outward current could be explicitly determined. The latter method offered the advantage that submembrane Ca^{2+} was better defined.

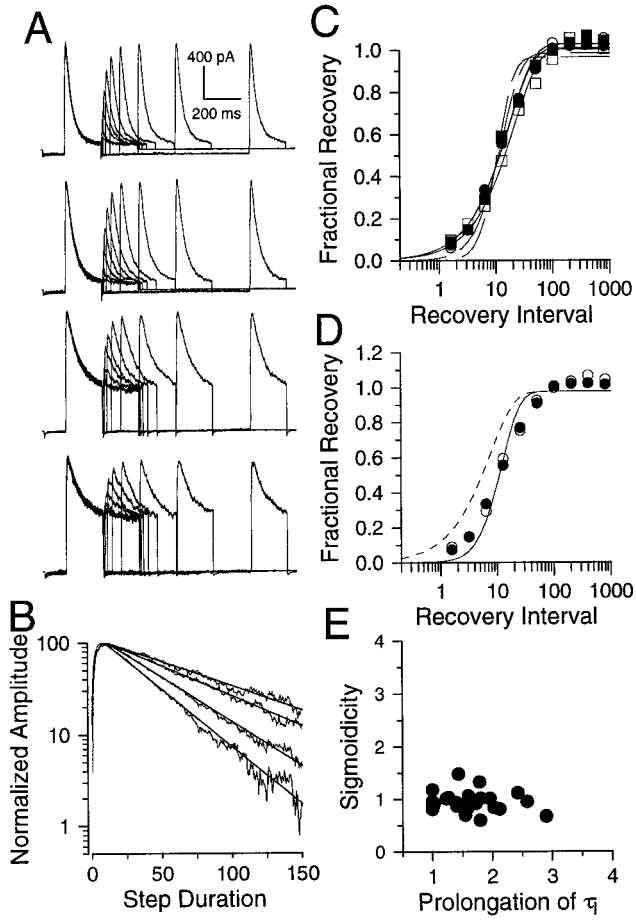

FIGURE 9 Trypsin removal of inactivation does not influence the rate of recovery from inactivation. Recovery from inactivation was defined with the paired pulse protocol shown in *A*. Pairs of 200-ms depolarizing steps to +60 mV were separated by 1.5-ms to 800-ms steps to −140 mV. A 100 ms step to −140 mV preceded the first step to +60 mV to remove resting inactivation at the holding potential (−60 mV). The patch was bathed with 10 μM Ca^{2+}, and patches with large, undefined numbers of channels were selected so that minimal averaging would be required in the recovery protocols. For the examples shown, 20 sweeps were used for each pulse-pair average. From top to bottom, traces show currents before and after each of three brief applications of trypsin to the patch. (*B*) The normalized inactivation time course for each of the currents in *A* is plotted, along with the best fit of a single exponential function (35, 45, 67, and 83 ms for control and subsequent trypsin applications, respectively). Current values for the last 100 ms of the second step to +60 mV after the 1.5-ms recovery interval were used to better define the exponential decay time course. (*C*) The fractional recovery as a function of recovery time is plotted for the set of traces in *A*. Single exponential functions are fit through the recovery points: 17.3 ms (control, ●); 17.8 ms (first trypsin, ○); 18.0 ms (second trypsin, ■); 21.3 ms (third trypsin, □). Fractional recovery was defined as $(P2_{max} - P1_{min})/(P1_{max} - P1_{min})$, where $P1_{min}$ refers to the final current level at the end of the first depolarizing step to +60, and $P1_{max}$ and $P2_{max}$ refer to maximum current amplitudes during the first and second depolarizing steps, respectively. Fits to the control recovery time course of the following function: $N(t) = N^*_{max}(1 - \exp(-t/\tau_r))^n$ where N_{max} and τ_r were free parameters, and $n - t/\tau_r$ was constrained to either two or four inactivation domains, are plotted as dotted lines. (*D*) The fractional recovery for the control and after the second trypsin application is shown. The solid line represents the best fit of Eq. 1 with a sigmoidicity term of 2.5. This fit yields a time constant of recovery of 7.65 ms and fails to describe the recovery time course. Assuming that the action of trypsin is to reduce the average number of inactivation particles in the population of channels, the predicted recovery time course when the average number of particles reaches 1, but assuming the same microscopic recovery rate, is shown for the dotted line. As inactivation is removed by trypsin, there is no indication of either changes in time constant or in sigmoidicity that would suggest that multiple domains must each dissociate during the recovery process. (*E*) The apparent sigmoidicity in the recovery from inactivation is plotted as a function of fractional prolongation of τ_i during trypsin-induced removal of inactivation for a set of seven cells. The recovery time courses, as in *C*, were fit with the equation above, but with *n* as an additional free parameter.

In Fig. 10, currents activated with and without extracellular 1.8 mM Ca^{2+} and with and without CTX are shown for a cell with BK_s current (Fig. 10 *A*) and a cell with BK_i current (Fig. 10 *B*). In both cases, a depolarizing command step to −9 mV was used to activate Ca^{2+} current and produce robust elevations of cytosolic Ca^{2+}. A subsequent step to +81 mV was then used to activate BK current relatively free of contamination by other currents. The middle pair of traces in each case show the outward current activated before, during, and after the removal of Ca^{2+}. The bottom traces show current before, during, and after the application of 100 nM CTX. For the cell with BK_s current, CTX blocks virtually all of the Ca^{2+}-dependent outward current. For the cell with BK_i current, 100 nM CTX blocks ~50% of the Ca^{2+}-dependent current. In Fig. 10, *C* and *D*, the time course of onset of block and recovery during CTX applications is plotted for the two cells shown in Fig. 10, *A* and *B*. The time course of onset and recovery from block was fit with a simple first-order blocking model to obtain estimates of the K_d of block. For cells with predominantly noninactivating current ($\tau_i > 110$ ms), the estimated K_d was 6.9 ± 2.3 nM, within the range of estimates of the effectiveness of CTX against BK channels in other studies (Miller et al., 1985; Park and Miller, 1992). In contrast, the sensitivity of BK_i current to CTX exhibited considerable variability. For the example shown, the apparent K_d for block was 62.7 nM.

Fig. 10 *E* illustrates the variability in CTX effectiveness in blocking BK current in chromaffin cells. For each cell, τ_i was determined and an estimate of the K_d of CTX block was obtained by fitting the time course of current block at one or more [CTX]. Whereas relatively sustained BK current was almost completely blocked by 100 nM CTX, cells with inactivating BK current exhibited considerable variability in sensitivity to CTX. For this set of cells, cells were grouped into those with τ_i values less than 60 ms, those with $60 < \tau_i < 110$ ms, and $\tau_i > 110$ ms. Cells with no BK inactivation were included in the latter group. When the mean τ_i for each group is plotted versus the estimated K_d for CTX blockade (Fig. 10 *E*), there is a strong inverse correlation between the rate of inactivation and CTX sensitivity. Thus cells with faster inactivating BK current tend to be more resistant to blockade by CTX.

The CTX sensitivity of BK current activated by voltage steps with 10 μM pipette [Ca^{2+}] was also examined, by using sequential applications of multiple CTX concentrations (Fig. 11) or by application of single concentrations. Currents were activated by steps to +90 mV with 10 μM

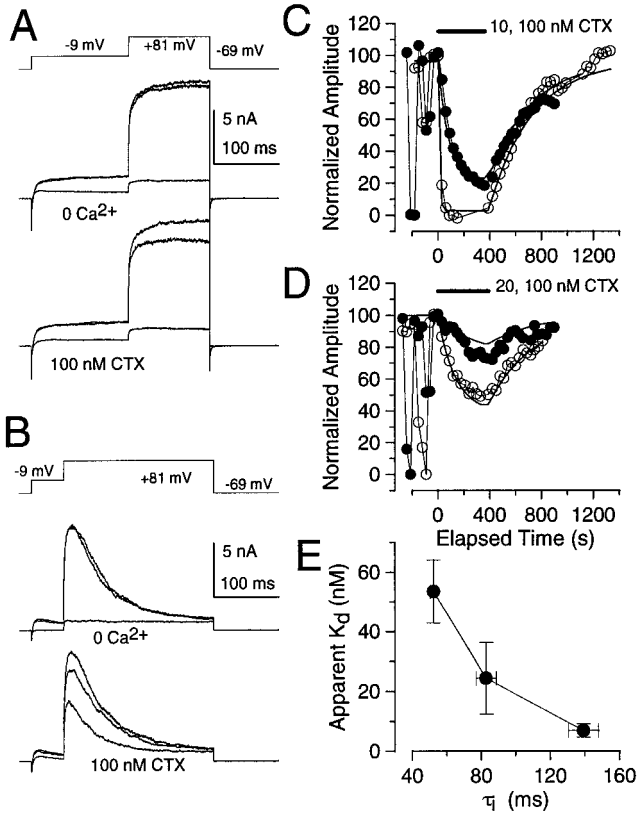

FIGURE 10 The sensitivity of BK_i current to CTX in perforated-patch recordings. (*A* and *B*) Outward current was elicited by a voltage-step to +81 mV after a loading step to −9 mV from a holding potential of −69 mV. The inward Ca^{2+} current activated at −9 mV produced a robust activation of BK during the subsequent step to +81 mV. In *A*, traces for a cell with BK_s current are shown (R_s = 10 MΩ; C_m = 5.8 pF) and, in *B*, traces for a cell (R_s = 12 MΩ; C_m = 9.4 pF) with BK_i current are shown. Traces marked 0 Ca^{2+} shows that most outward current activated at +81 mV is dependent on Ca^{2+}. On the bottom, currents before, during, and after the application of 100 nM CTX are shown. CTX at a concentration of 100 nM blocks almost all Ca^{2+}-dependent BK_s current. In *B*, 100 nM CTX blocks only about half of the Ca^{2+}-dependent BK_i current. (*C* and *D*) The time course of reduction of peak outward current for the cells in *A* and *B* is plotted in each case for two CTX applications (*C*, 10 and 100 nM; *D*, 20 and 100 nM). The time of washout of drug was adjusted to be identical. Lines are the best fit of a simple blocking model with onset and recovery at both concentrations fit simultaneously in both cases. Reductions of current before CTX application were either to 0 Ca^{2+} (~100% reduction) or 300 μM TEA (~50% reduction), showing the time course of fast block relative to CTX action. For the BK_s cell, the resulting K_d of block was 2.7 nM, whereas for the BK_i current it was 62.7 nM. (*E*) The estimated K_d for CTX block for three groups of cells is plotted as a function of the mean τ_i for each group. The groups were those with $\tau_i < 60$ ms, those with $60 < \tau_i < 110$ ms, and those with $\tau_i > 110$ ms.

pipette Ca^{2+} in a cell with primarily BK_i current (Fig. 11 *A*) and a cell with primarily BK_s current (Fig. 11 *B*), before and during application of CTX. Fig. 11, *C* and *D*, plots the time course of block and the fit of a simple block model for both cells, and Fig. 11 *E* provides a concentration-response curve for CTX blockade. For seven cells with predominantly BK_s current, the estimated K_d was 3.3 ± 1.1 nM. For 26 cells with predominantly BK_i current, the estimated K_d was 21 ± 15 nM.

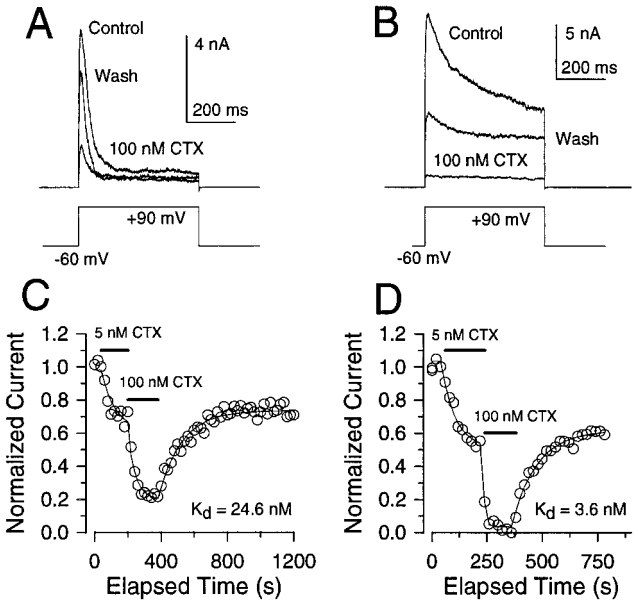

FIGURE 11 Blockade by CTX of BK current activated by 10 μM pipette Ca^{2+}. (*A*) BK_i currents activated by voltage steps to +60 mV before, during, after 100 nM CTX are shown. (*B*) Predominantly BK_s currents activated by voltage steps to +60 mV before, during, after 100 nM CTX are shown. (*C*) The amplitude of peak current as a function of elapsed time for the cell shown in *A* is plotted along with a fit of a simple blocking model with K_d = 24.6 nM. (*D*) The amplitude of peak current as a function of elapsed time for the cell shown in *B* is plotted, along with a fit of a simple blocking model, with K_d = 3.6 nM.

Trypsin-mediated removal of inactivation does not alter the sensitivity of BK_i current to CTX

The apparent difference in sensitivity to CTX between BK_i and BK_s current might reflect some structural or functional difference between channel variants that arises from the presence of functional inactivation domains. To test this possibility, the CTX sensitivity of BK current was examined during the trypsin-mediated removal of inactivation. As in Figs. 5 and 6, trypsin was introduced into cells through the recording pipette. Fig. 12 *A* shows the typical removal of inactivation by trypsin. Application of 100 nM CTX after inactivation has been removed results in only a partial block of BK current (Fig. 12, *B* and *D*). A fit to the onset and recovery from CTX blockade yielded an estimated K_d of 69 nM (Fig. 12 *C*). Similar results were obtained from two other cells, indicating that BK_i channels with inactivation removed remain relatively resistant to blockade by CTX.

The current inactivation rate is faster during blockade by CTX

Blockade of BK_i current by CTX is consistently associated with an increase in inactivation rate of the residual unblocked current (Fig. 13). In Fig. 13 *A*, BK_i current traces before, during, and after application of 100 nM CTX are shown. In Fig. 13 *B*, normalized current before and during

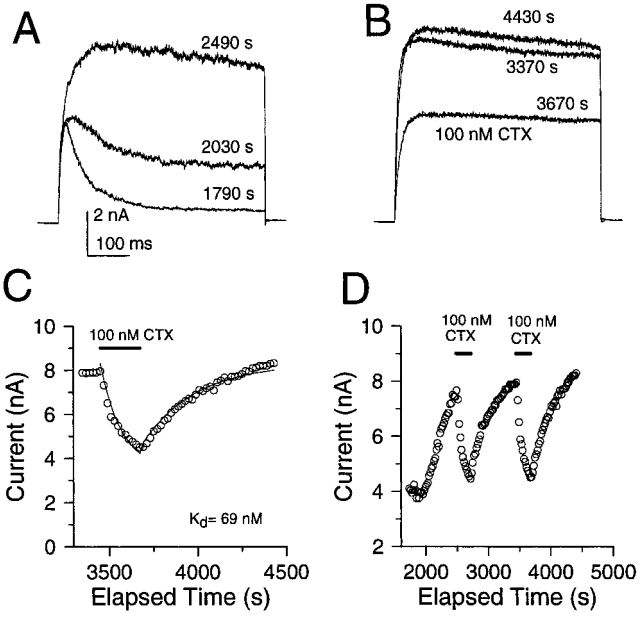

FIGURE 12 Removal of inactivation by trypsin does not diminish the resistance of BK_i current to blockade by CTX. (*A*) Currents elicited by steps to +60 mV after a 100-ms step to −140 mV with 10 μM pipette Ca^{2+} are shown at different times after the introduction of trypsin into the cytosol. The holding potential between steps was −60 mV. By ~2500 s, inactivation is largely removed. (*B*) Currents before, during, and after application of 100 nM CTX are shown. (*C*) Time course of block onset and recovery for the second CTX application fit to the simple block model yielding an effective K_d of 69 nM. (*D*) The peak current amplitude as a function of elapsed time is plotted, showing the effects of two different applications of 100 nM CTX.

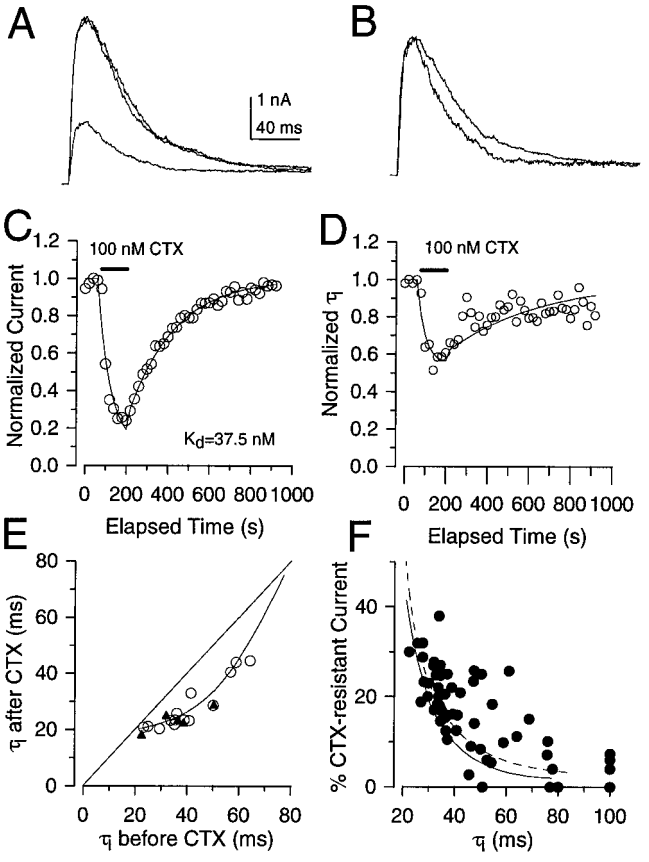

FIGURE 13 In the presence of CTX, the rate of inactivation of residual, unblocked BK_i current is faster. (*A*) Currents activated by a step to +60 mV after a 100-ms step to −140 mV with 10 μM pipette Ca^{2+} are shown for cases before, during, and after the application of 100 nM CTX. (*B*) Normalized currents from before and during CTX application are shown to emphasize the difference in inactivation rate in the presence of CTX. The control τ_i was ~34 ms, whereas in 100 nM CTX, $\tau_i \approx 20$ ms. (*C*) The time course of peak current reduction and recovery from CTX is plotted along with the fit of a simple block model with a K_d of 37.5 nM. (*D*) The normalized changes in τ_i are plotted for the same set of currents. In the presence of CTX, the inactivation rate is 40% faster and the rate gradually returns to normal values after the removal of CTX. (*E*) τ_i measured in the presence of 100 nM CTX is plotted as a function of the initial τ_i for several cells. CTX tends to produce larger changes in the inactivation rate in cells with slower initial τ_i. CTX tends to have minimal effects on τ_i in cells with initial τ_i approaching ~20–25 ms. The theoretical curve is the predicted relationship, assuming a τ_{min} of 20 ms. Solid triangles show values obtained from outside-out patches. (*F*) The residual unblocked BK current in the presence of 100 nM CTX is plotted as a function of the initial τ_i of the cell. The solid line was obtained from simulations of currents based on different mole fractions of bk_i subunits, assuming a minimum τ_i of 20 ms. Values for K_{d1} of 2 nM and for K_{d2} of 100 nM were used. A somewhat slower minimum τ_i (25 ms) yields a stronger correspondence (*dotted line*) with the observed trend in the experimental observations.

CTX application is plotted to emphasize the change in τ_i during CTX. In Fig. 13 *C*, the time course of block of peak current by 100 nM CTX is plotted, yielding an estimated K_d of 37.5 nM. For each current trace, the current decay was fit with a single exponential, and the normalized τ_i is plotted as a function of elapsed time in Fig. 13 *D*. In this case, the inactivation decay rate almost doubled in the presence of 100 nM CTX. The effects of 100 nM CTX on BK current elicited by 10 μM Ca^{2+} were also examined in outside-out patches (data not shown). As with whole-cell experiments, 100 nM CTX produced variable blockade of peak BK_i current and, in all cases ($n = 6$), τ_i was faster in the presence of CTX (Fig. 13 *E*).

We feel it simplest to propose that the effects on τ_i result from selective deletion by CTX of those channels containing CTX-sensitive subunits. The remaining unblocked channels would then have, on average, more inactivation-competent, bk_i subunits, resulting in the observed increase in the macroscopic inactivation rate. An additional prediction of this model is that there should be some correlation between the initial τ_i and the τ_i after blockade by CTX. The predicted correlation, in this case calculated assuming a τ_{min} of 20 ms, and actual observed values are plotted in Fig. 13 *E*. The agreement seems reasonable. In addition to the expected relationship between changes in τ_i and the initial τ_i, it is expected that the amount of block of peak BK_i current will also exhibit a correlation with the initial τ_i. Cells with faster initial inactivation rates are expected to have less total block by CTX. The predicted relationship between the fractional block by 100 nM CTX and the initial τ_i in a cell is plotted in Fig. 13 *F*. Although the predicted relationship depends significantly on K_{d2} (the CTX sensi-

tivity of channels with four bk_i subunits) and the hypothesis that the channel population really follows a binomial distribution, the general trend in the experimental estimates seems adequately consistent with the heteromultimer hypothesis.

The frequency of occurrence of noninactivating channels in patches is consistent with heteromultimer formation

Results above suggest that most BK channels in cells with inactivating BK current may have fewer than four inactivation domains. Thus, if chromaffin cell BK channels arise from the heteromultimeric assembly of inactivation-competent bk_i subunits and CTX-sensitive bk_s subunits, we would expect that BK_s channels should be found to some extent in patches with BK_i channels, but only at frequencies that reflect the average number of inactivation domains per channel in the cell. For example, if cells with BK_i current contain, on average, two inactivation domains per channel, the prediction of the random, independent binomial assembly of separate bk_i and bk_s subunits is that one out of 16 BK channels will be noninactivating. If, on average, there are three inactivation domains per channel, the binomial prediction is that only about one out of 256 BK channels will be noninactivating.

Here, to better define the true number of channels in a given patch, each voltage step used to activate BK channels was preceded by a 200-ms hyperpolarizing conditioning step to −140 mV (e.g., Fig. 2 *A*). The step to −140 mV with 10 μM Ca^{2+} ensures that most channels are available for activation during the subsequent activation step (Ding et al., 1996), whereas the activation step to +60 mV results in a near-maximum open probability (Prakriya et al., 1996). Patches were considered to have a BK_s channel, if a channel remained open at the end of the command step (400 ms) in over 90% of the sweeps. With a time constant of inactivation of 100 ms, a BK_i channel will be open at the end of a 400-ms voltage step in only ~1.8% of the sweeps. If a patch contains 20 BK_i channels, one BK_i channel would therefore be expected to be open at 400 ms in only ~37% of the sweeps. For the set of patches examined here, the slowest time constants were always faster than 75 ms, and the patches examined always contained less than 20 BK_i channels. Thus, if one and only one channel is open more than 90% of the time at the end of a sweep, the patch probably contains only a single BK_s channel. Although it is possible in an isolated case that a BK_i channel may be open at the end of the 400-ms voltage step, it is very unlikely that a BK_i channel will be open at the end of 90% of the voltage steps. The estimate of the maximum number of channels in the patch was then taken from the activation step that activated the maximum number of channels. In seven of eight cases where trypsin was subsequently used to remove inactivation, the estimate of the maximum number of channels in the patch obtained after trypsin agreed with that taken from the peak number of channels open before trypsin.

A summary of the occurrence of BK_i and BK_s channels for a set of 53 patches is provided in Table 1. Two patches were observed that contained BK_s channels exclusively, one with six channels and one with one channel. Forty-four patches contained BK_i channels exclusively, and seven patches, although containing predominantly BK_i channels, also contained at least one BK_s channel. For all patches with BK_i channels, a total of 8 BK_s channels and 321 BK_i channels were observed. Thus, ~2.4 out of every 100 channels were BK_s channels. If, over the entire population of cells with BK_i current, the ratio of bk_i and bk_s subunits were similar, this would be consistent with there being ~2.4 inactivation domains per channel. However, the trypsin and CTX experiments suggest that the ratio of bk_i to bk_s subunits may not be uniform among all cells with phenotypically inactivating current. If we assume that there were no BK_s channels in those cells from which the patches contained only BK_i channels, then 8 BK_s channels were observed out of a total of 89 channels (8.9 BK_s per 100 channels). This would provide an upper limit for the frequency of occurrence of BK_s channels in cells with predominantly BK_i channels, which corresponds to an average of a little more than 1.8 inactivation domain per channel.

If the presence of BK_s channels in patches with mostly BK_i channels truly reflects the availability of two different channel subunits for assembly into heteromultimers, we would expect that τ_i should, on average, be slower for patches that contain BK_s subunits, because such cells may have fewer inactivation domains per channel. This analysis, which was limited to the 31 patches that contained at least five channels, is summarized in Table 2. Patches were separated into five groups by τ_i. For seven patches with τ_i faster than 30 ms, no BK_s channels were observed out of 57 BK_i channels. In contrast, for 10 patches with τ_i slower than 50 ms, 6 BK_s channels were observed out of a total of 99 channels. This latter frequency agrees with an average of ~2 inactivation domains per channel. For patches with τ_i between 30 and 50 ms, 2 BK_s channels were observed out of a total of 123 channels, consistent with a prediction of ~2.5–2.6 inactivation domains per channel.

TABLE 1 Occurrence of BK_i and BK_s channels in patches

	patches	N_{BK_s}	N_{BK_i}	f	IDs
Totals	53	15	321	0.047	~2.2
Patches with only BK_s channels	2	7	0	1.0	0.0
Patches with at least one BK_i channel	51	8	321	0.024	~2.4
BK_i patches with or without BK_s channels					
BK_i/BK_s	7	8	81	0.090	1.8–1.9
BK_i alone	44	0	240	0.0	4.0

N_{BK_i}, Number of BK_i channels; N_{BK_s}, number of BK_s channels; f, frequency of occurrence of BK_s channels; IDs, the predicted average number of inactivation domains per channel, given the frequency of occurrence of totally noninactivating channels, assuming the binomial model for assembly of two independent subunits, with one bk_i subunit being sufficient for inactivation.

TABLE 2 Patches with five or more channels

Total	Patches with BK_s alone		Patches with BK_i alone		BK_i patches with one BK_s channel		BK_i patches with two BK_s channels
32	1		24		6		1
N_p	N_c	N_{BK_i}	N_{BK_s}	τ_i (ms)	SD	$\%BK_s$	IDs
1	6	0	6	—	—	100.0	0
6	51	48	3	70.4	5.5	5.88	2.0–2.1
5	48	45	3	54.0	2.9	6.25	2.0
7	72	71	1	45.3	2.7	1.39	2.6–2.7
6	51	50	1	37.3	0.95	1.96	2.5
7	57	57	0	24.4	2.0	0	4.0
Totals excluding single BK_s patch							
31	279	271	8	45.3	16.0	2.87	2.3–2.4

N_p, Number of patches; N_c, number of channels; N_{BK_i}, number of BK_i channels; N_{BK_s}, number of BK_s channels; τ_i, mean inactivation time constant for set of patches; SD, standard deviation of mean time constant; $\%BK_s$, percentage of BK_s channels in set of patches; IDs, as in Table 1.

Accounting for the diversity in macroscopic BK phenotype in rat chromaffin cells

The results to this point provide a set of independent observations that are each generally consistent with the heteromultimer hypothesis presented in Fig. 1. As an additional test of this model, we examine the extent to which this single model accounts not only for the rate and amount of inactivation among a set of cells, but also properties of block by CTX in the same set of cells. For each cell, currents were recorded in normal saline and in the presence of 100 nM CTX. The cells illustrated in Fig. 14 were chosen to represent the range of current behaviors that can be observed. Current waveforms were fit with the Hodgkin-Huxley activation-inactivation model described in Materials and Methods and previously used in Fig. 7. In this case, current remaining at the end of a voltage step in the presence of 100 nM CTX was used to constrain I_{KV}. In cases where inactivating current persisted in the presence of 100 nM CTX (e.g., Fig. 14, *C* and *D*), τ_i of the residual current strongly defined the limiting τ_{min} expected for channels with four inactivation domains. Currents before and in the presence of CTX were fit simultaneously, using time and CTX concentration as two independent variables. Thus, for each pair of traces (control and 100 nM CTX) shown in Fig. 14, the same set of activation and inactivation parameters was used, with the simple addition that differential blockade of bk_i and bk_s subunits by CTX was considered. For the examples shown, K_{d1} and K_{d2} were constrained to 3 nM and 100 nM, respectively, although K_{d2} was not well defined when used as a free parameter. For all cells, this fitting procedure yields a limiting τ_{min} between 19 and 30 ms, despite the wide range in observed macroscopic current decay time constant and amount of persisting steady-state current. This limiting minimum τ_i is qualitatively consistent with other observations, including the limiting τ_i observed in single channels (Fig. 2), and with the increase in inactivation rate with CTX (Fig. 13). Thus both the amount of reduction of current by CTX and the changes in apparent τ_i produced by CTX are well described over a range of BK current phenotypes. The diversity of current phenotypes can be described simply by changing the mole fraction of bk_i subunits within the cell, without substantial alteration of any other parameters.

DISCUSSION

The results show that 1) removal of inactivation by trypsin both in patches and in cells is best accounted for by an average of two to three native inactivation domains per channel; 2) cells predicted to have, on average, more inactivation domains per channel have faster inactivating BK_i current; 3) BK_i current exhibits a range of sensitivities to CTX, with greater CTX resistance associated with faster BK current inactivation; 4) CTX blockade results in an increase in BK_i inactivation rate; 5) noninactivating BK_s channels are found at a low frequency in patches with inactivating BK channels and, furthermore, BK_i channels in patches with a BK_s channel inactivate, on average, more slowly than BK_i channels in patches without BK_s channels.

To account for this set of observations, we assume that both BK_i and BK_s channels arise from *Slo* subunits and that BK channels are tetramers. Each of the observations just described can be accounted for by the model presented in Fig. 1, namely that BK_i current represents the ensemble behavior of four distinct stoichiometric assemblies of two distinct BK subunits, one that confers inactivation behavior (bk_i), and one that does not participate in inactivation (bk_s).

Recently the existence of two distinct *Slo* splice variants in chromaffin cells has been described (Saito et al., 1997). One variant encodes a unique cysteine-rich, 59-amino acid insert similar to a variant also found in pancreatic β cells (Ferrer et al., 1996), which also express inactivating BK channels (Lingle et al., 1996). Although expression of a *Slo* construct containing this insert does not produce inactivating BK currents in *Xenopus* oocytes (Saito et al., 1997), it was proposed that this splice variant may be a specific component of BK_i channels. In the absence of a specific, inactivation-competent BK subunit, the possibility must

also be considered that inactivation may arise from the specific association of a critical accessory subunit with the channel complex. The predictions of the model of heteromultimeric assembly are essentially equivalent, irrespective of whether inactivation is intrinsic to a particular subunit or a given subunit simply anchors the association of a specific inactivation-competent accessory subunit, analogous to inactivation-competent accessory subunits of some voltage-dependent K^+ channels (Rettig et al., 1994; Morales et al., 1995).

Implications concerning the mechanism of BK_i inactivation

Inactivation of many voltage-dependent channels involves key cytosolic structures, which in many cases exhibit sensitivity to peptidase action (Armstrong et al., 1973; Gonoi and Hille, 1987; Gomez-Lagunas and Armstrong, 1995). Similar to voltage-dependent K^+ channel inactivation mediated by N-terminal structures, BK_i inactivation is slowed by trypsin. This result strongly argues that multiple cytosolic structures are available to produce inactivation of BK_i channels. The up to fourfold prolongation of inactivation by trypsin suggests that one of up to four independently acting cytosolic structures is sufficient to produce inactivation. The gradual slowing of inactivation by trypsin also argues against a mechanism involving the concerted action of multiple domains, where all domains must be intact for the channel to inactivate. This interpretation is also supported by the lack of effect of trypsin on recovery from inactivation and the single exponential nature of the recovery time course—dissociation of a single particle appears sufficient to produce recovery from inactivation. Because of the tetrameric nature of voltage-dependent K^+ channels (MacKinnon, 1991) and BK channels (Shen et al., 1994), the simplest view is that inactivation involves up to four distinct inactivation domains, one per channel monomer, each of which can act largely independently to produce inactivation.

Despite the absence of structural information on this issue, the results argue for a rather conventional view of BK_i inactivation, with similarity to N-terminal inactivation of voltage-dependent K^+ channels. However, this contrasts with other aspects of BK_i inactivation. Specifically, cytosolic channel blockers, such as TEA, QX-314, and the *Shaker*B ball peptide, fail to retard the inactivation process (Solaro et al., 1997), suggesting that the occupancy of pore blocking sites on the cytosolic side of the channel does not prevent movement of the native inactivation domains to their blocking sites. As a consequence, it has been proposed that the cytosolic structure preventing ion permeation during inactivation may occlude the channel at some distance from the mouth of the pore (Solaro et al., 1997).

Trypsin-induced slowing of BK_i inactivation: involvement of fewer than four cytosolic domains?

The present results suggest that, although BK_i channels may contain up to four inactivation domains, on average there are only two to three inactivation domains per BK_i channel in most rat chromaffin cells. This is supported most directly by the extent of slowing of inactivation rates, both in

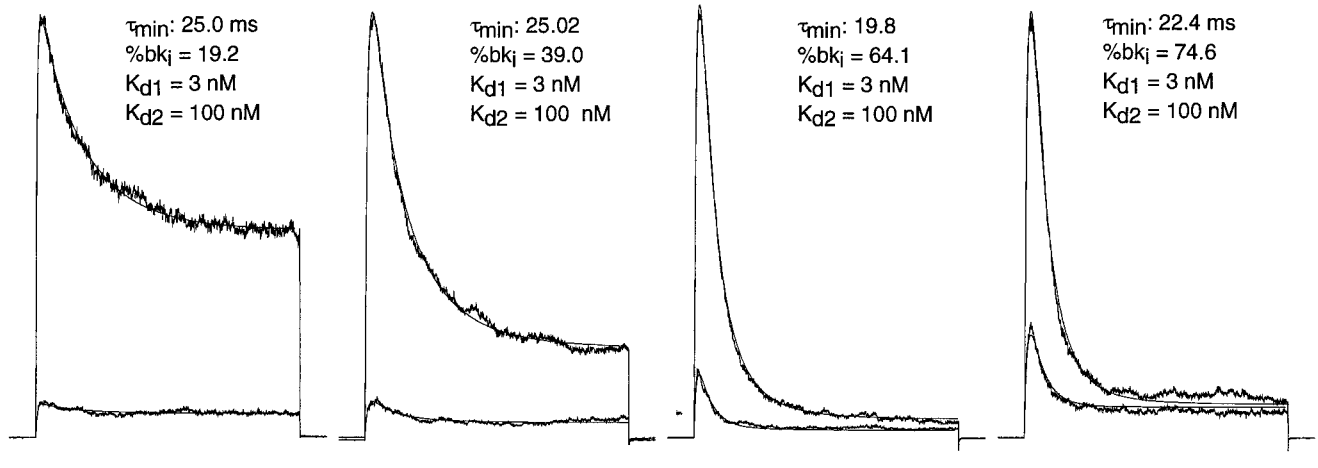

FIGURE 14 Aspects of the blockade of BK_i current by CTX and diversity in BK current phenotype can be described by the heteromultimer hypothesis. Current waveforms elicited by voltage steps to +60 mV with 10 μM pipette [Ca^{2+}] are shown for four separate rat chromaffin cells. The steps to +60 mV were preceded by a 100-ms step to −140 mV from a holding potential of −60 mV. Each pair of traces shows currents with normal 0 Ca^{2+} extracellular saline, with or without 100 nM CTX. Most rat cells exhibit behavior more similar to that seen for the two right-hand cells, with far fewer cells exhibiting the less pronounced inactivation seen for the two left-hand cells. The residual current at the end of the voltage step in the presence of CTX was assumed to be contaminating non-BK current and was assumed to be identical before and after CTX. Each pair of traces was fit simultaneously with K_{d1} and K_{d2} constrained to 3 nM and 100 nM, respectively, such that the same set of parameters for activation, inactivation, and mole fraction bk_i subunits was required to account for each pair of traces. Fit parameters were (*A*) I_{max} = 104.7; τ_a = 2.5 ms, n = 1.2, τ_{min} = 25.0, bk_i% = 19.2; (*B*) I_{max} = 132.2, τ_a = 5.8 ms, n = 1.0, τ_{min} = 25.0 ms; bk_i% = 39.0; (*C*) I_{max} = 168.8, τ_a = 6.3 ms, n = .9, τ_{min} = 19.8 ms, bk_i% = 64.1; (*D*) I_{max} = 174.9, τ_a = 7.8 ms, n = 0.9, τ_{min} = 22.4 ms, bk_i% = 74.6.

ensembles of openings in patches and in cells perfused with trypsin or papain. In addition, the relationship between f_{ss} and τ_i, particularly at early times in the trypsin digestion, and changes in the current waveform during the trypsin digestion process strongly suggest that inactivation involves fewer than four inactivation domains per channel. Although a direct measure of the limiting τ_i after prolonged enzymatic digestion in theory should also help define the average number of inactivation domains per channel, at long digestion times slow components of inactivation were observed, which resulted in marked deviation from the predictions of any simple multiple, independent domain inactivation mechanism.

Several other factors might also complicate the interpretation of changes in τ_i and f_{ss} with trypsin. If there were steric hindrance among individual inactivation domains during the inactivation process, the relationship between prolongation in τ_i and f_{ss} would be unable to distinguish between fewer than four inactivation domains per channel or steric interactions. Another factor that might compromise the predicted relationship between τ_i and f_{ss} is that digestion by trypsin may not result in a strictly binomial distribution of channels within the population. Specifically, it is possible that once one inactivation domain is attacked by trypsin, attack at other subunits of the same channel may be more likely, either because of removal of some steric hindrance or because of more favorable positioning of a trypsin molecule for subsequent attack. This scenario would result in smaller predicted changes in τ_i relative to changes in f_{ss}, although limiting values of τ_i should be similar in either case.

We feel that none of these factors are likely explanations of the results. Although steric hindrance between inactivation domains would explain the less than fourfold prolongation of τ_i in most cells, the observed variability in estimates of average number of inactivation domains would seem more consistent with diversity in average BK_i channel composition. Similarly, the observed dependence of the estimates of average number of inactivation domains on initial τ_i is not explained by steric hindrance. The possibility of nonbinomial distributions among particular subunit stoichiometries during the digestion process is also inconsistent with the curvature, early in the digestion process, observed in the relationship between the prolongation of τ_i and f_{ss}. Specifically, the large change in τ_i relative to f_{ss} would not be expected. Furthermore, other results, including the frequency of occurrence of BK_s channels and the variability in CTX sensitivity, appear to provide independent support for the idea that there is variability in the subunit composition of BK_i channels.

What is the basis for the relative resistance to CTX of BK_i channels?

The inverse correlation of CTX sensitivity and inactivation behavior suggests that there is some structural difference between BK_i and BK_s channels on the extracellular side of these channels. The simplest interpretation might be that the two distinct subunits contributing to BK_i channels differ in critical residues near the pore that influence CTX binding. Previous studies of blockade of *Shaker* K^+ channels by CTX have generated a map of both channel residues and toxin residues that are likely to participate in toxin binding (Stampe et al., 1994; Goldstein et al., 1994). However, the homologous regions of known *Slo* peptides contain no alternative splice variation that would be expected to influence interaction with toxin (Adelman et al., 1992; Butler et al., 1993; Pallanck and Ganetsky, 1994; Tseng-Crank et al., 1994). Thus this explanation would require that an unknown BK homolog be present in chromaffin cells that has not been identified in previous work (Saito et al., 1997). Although CTX-resistant BK channels from brain membranes have also been studied in lipid bilayers (Reinhart et al., 1989), we are unaware of any reports of CTX resistance among BK channels in native cells.

Several lines of investigation suggest that factors besides α-subunit sequence may also influence toxin sensitivity. For example, CTX binding may also be influenced by a β-subunit, when present. In initial attempts to isolate BK channel proteins, CTX was found to covalently attach to the β-subunit (Knaus et al., 1994a,b). In recent work there is some suggestion that β-subunit-containing channels are somewhat less sensitive to blockade by CTX (Dworetsky et al., 1996), but this issue will require further study. The possibility must also be considered that alterations in cytoplasmic channel domains may subtly influence structural aspects of extracellular domains. A 10-fold slowing in the rate of toxin association represents only a small change in the availability of target channel residues. Thus a change in toxin sensitivity may not require that extracellularly exposed residues of the channel α-subunits differ between bk_i and bk_s subunits. The lack of effect of removal of inactivation on the sensitivity of BK_i currents to CTX implies that whatever is responsible for the relative resistance to CTX is not substantively altered by removal of the inactivation process itself.

Diversity of BK channel phenotype in rat chromaffin cells

In previous work, we indicated that ~80% of rat chromaffin cells express predominantly BK_i currents, whereas the remainder expressed noninactivating or more slowly inactivating BK currents (Solaro et al., 1995). This corresponded well with the frequencies of occurrence of patches that expressed almost exclusively BK_i channels and those that expressed either BK_s channels or a mix of BK_i and BK_s channels. Our present results are in general accord with earlier observations, but provide a more detailed picture of the possible mechanisms underlying the relative occurrence of BK_i and BK_s channels. Experiments described here indicate that, even within the population of cells in which BK current exhibits almost complete inactivation, there is some diversity in phenotypic properties in terms of inactivation

rates and CTX sensitivity. A question that arises is the following: Are those cells that exhibit essentially noninactivating BK current a distinguishable subpopulation of chromaffin cells or simply one extreme on a continuum of a homogeneous population? Specifically, we wish to consider the possibility that apparent diversity may arise simply from the normal differential expression of two channel subunits in an essentially homogeneous population of cells.

The hypothesis that heteromultimeric assembly of two distinct subunits may account for BK current behavior in chromaffin cells has several interesting functional implications. First, because the presence of a single bk_i subunit in a channel is sufficient to confer full inactivation on that channel (bk_i subunits are essentially phenotypically dominant), the existence of some cells in which there is essentially no BK_i current argues that those cells must express bk_i subunits at negligible levels. Second, several lines of evidence presented above suggest that, in cells and patches with predominantly BK_i current, the mole fraction of bk_i subunits may be as low as 0.5 in many cells (i.e., ~2 inactivation domains per channel) or as high as ~0.7 (i.e., ~3.1–3.2 inactivation domains per channel). Thus, although bk_i subunits appear to be absent in some cells, this analysis would suggest that reasonable levels of bk_s subunits may be present in all cells.

We imagine two sorts of explanations to account for the range of current behaviors. In one case, cells expressing solely bk_s subunits represent a distinct subpopulation of chromaffin cells, whereas the other chromaffin cells express both bk_i and bk_s subunits, resulting in current phenotypes reflecting some normal variability in relative subunit expression among a cell population. In the second case, both BK_i and BK_s phenotypic variants may arise as the consequence of normal variability in relative subunit expression among a biochemically homogeneous cell population. Although there is an absence of information about the distribution in copy numbers of any protein within an essentially homogeneous cell population, some variation in expression levels would certainly be expected. For two peptides whose levels are independently regulated or whose levels are perhaps inversely regulated (e.g., different splice variants), mole fraction ratios spanning a quite broad range are to be expected.

Assuming that the expression levels of two subunits within a population of cells vary in a Gaussian fashion, but independently of each other, we calculated the expected fraction of current that is totally inactivating for each cell within the cell population (results not shown). Even at relatively high average mole fractions of bk_i subunits within the population, occasional cells will be encountered that express predominantly BK_s current. This indicates that what may appear to represent clear phenotypic heterogeneity among cells may, in fact, simply represent the extremes of a spectrum of behavior arising from a homogeneous cell population. If the mole fractions of the two critical subunits are inversely correlated, as perhaps for two different alternative splice variants, the tendency to observe phenotypic extremes based on a Gaussian distribution of one subunit will be even greater. Thus these considerations suggest that the existence of phenotypic extremes in a cell population as observed both here and in our earlier work (Solaro et al., 1995) may be insufficient to argue for the existence of two subpopulations of cells.

Functional implications of heteromultimeric assembly of BK channels

Although heteromultimeric assembly of voltage-dependent K^+ channels has been demonstrated both with in vitro expression systems (Isacoff et al., 1990; Ruppersberg et al., 1990; Christie et al., 1990) and in native cells (Sheng et al., 1993; Wang et al., 1993), typically the functional properties of the heteromultimeric constructs differ only subtly from those of the parent homomultimeric constructs. In such cases, it has not been obvious what the functional significance of the heteromultimeric construct might be, although the existence of such constructs has been promoted as evidence of an additional mechanism by which K^+ channel diversity can be generated. In the present case, the putative coassembly of bk_i and bk_s subunits provides probably the most dramatic example of a range of functional diversity arising from heteromultimeric assembly.

Given the postulated role of BK current in chromaffin cells (Solaro et al., 1995) and in most neurons (Lancaster and Pennefather, 1987; Goh and Pennefather, 1987) in action potential repolarization, it is interesting to consider what the functional impact of this diversity might be. Even accounting for a faster inactivation rate at physiological temperatures, it is unlikely that significant inactivation of BK_i channels will occur during single action potentials (e.g., Solaro et al., 1995). However, earlier work indicated that BK_i and BK_s channels also differ in deactivation properties (Solaro et al., 1995). Furthermore, we expect that among cells with BK_i channels there will be differences in the steady-state inactivation behavior, depending on the average stoichiometry of BK_i channels within the cell. Thus we imagine that, as a consequence of the stoichiometry of the BK channel population, there may be a continuum of BK current availability and deactivation rates. The significance of such functional diversity in chromaffin cells remains obscure. However, within hair cells of the cochlea, it has been proposed that a range in properties of BK channels may underlie the range of frequency response exhibited across hair cells (Art and Fettiplace, 1987; Fuchs, 1992; Wu et al., 1995), a property critical to the electrical tuning properties of the hair cells. Rather than invoke a large number of splice variants to account for the range of BK properties in hair cells, the phenomenon observed here provides a relatively simple method by which a continuum of phenotypic variation in BK channel properties can be achieved. A similar heteromultimeric model for the assembly of BK channels from two distinct subunits has, in fact, been recently proposed for reptilian and avian cochleas (Wu

and Fettiplace, 1996). The present results provide experimental support for the idea that variation in BK channel properties, at least in some cells, may arise from this type of mechanism.

We thank S. Swanson for the preparation of chromaffin cells, Dr. C. R. Solaro for participation in the early stages of this work, and Drs. J. H. Steinbach and J. Nerbonne for comments on the manuscript.

This work was supported by DK-46564 from the National Institutes of Health.

REFERENCES

Adelman, J. P., K. Z. Shen, M. P. Kavanaugh, R. A. Warren, Y. N. Wu, A. Lagrutta, C. T. Bond, and R. A. North. 1992. Calcium-activated potassium channels expressed from cloned complementary DNAs. *Neuron.* 9:209–216.

Armstrong, C. M., F. Bezanilla, and E. Rojas. 1973. Destruction of sodium conductance inactivation in squid axons perfused with pronase. *J. Gen. Physiol.* 62:375–391.

Art, J. J., and R. Fettiplace. 1987. Variation of membrane properties of hair cells isolated from the turtle cochlea. *J. Physiol. (Lond).* 385:207–242.

Butler, A., S. Tsunoda, D. McCobb, A. Wei, and L. Salkoff. 1993. mSlo, a complex mouse gene encoding "maxi" calcium activated potassium channels. *Science.* 261:221–224.

Christie, M. J., R. A. North, P. B. Osborne, J. Douglass, and J. P. Adelman. 1990. Heteropolymeric potassium channels expressed in *Xenopus* oocytes from cloned subunits. *Neuron.* 2:405–411.

Covarrubias, M., A. Wei, and L. Salkoff. 1991. *Shaker*, Shall, Shab, and Shaw express independent K^+ current systems. *Neuron.* 7:763–773.

Ding, J. P., C. R. Solaro, and C. J. Lingle. 1996. The dependence of recovery from inactivation of BK channels in rat chromaffin cells on calcium and voltage. *Biophys. J.* 70:A192.

Dworetsky, S. I., C. G. Bossier, J. T. Lum-Ragan, M. C. Mckay, D. J. Post-Munson, J. T. Trojnacki, C.-P. Chang, and V. K. Gribkoff. 1996. Phenotypic alteration of a human BK(hslo) channel by *hSlo*β subunit coexpression: changes in blocker sensitivity, activation/relaxation and inactivation kinetics, and protein kinase A modulation. *J. Neurosci.* 16:4543–4550.

Fenwick, E. M., P. B. Fajdiga, H. B. S. Howe, and B. G. Livett. 1978. Functional and morphological characterization of isolated bovine adrenal medullary cells. *J. Cell Biol.* 76:12–30.

Ferrer, J., J. Wasson, L. Salkoff, and M. A. Permutt. 1996. Cloning of human pancreatic islet large conductance Ca^{2+}-activated K^+ channel (*hSlo*) cDNAs: evidence for high levels of expression in pancreatic islets, and identification of a flanking genetic marker. *Diabetologia.* 39:891–898.

Fuchs, P. A. 1992. Ionic currents in cochlear hair cells. *Prog. Neurobiol.* 39:493–505.

Goh, J. W., and P. S. Pennefather. 1987. Pharmacological and physiological properties of the afterhyperpolarization current of bullfrog ganglion neurones. *J. Physiol. (Lond.).* 394:315–330.

Goldstein, S. A. N., D. J. Pheasant, and C. Miller. 1994. The charybdotoxin receptor of a *Shaker* K^+ channel: peptide and channel residues mediating molecular recognition. *Neuron.* 12:1377–1388.

Gomez-Lagunas, F., and C. M. Armstrong. 1995. Inactivation in ShakerB K^+ channels: a test for the number of inactivating particles on each channel. *Biophys. J.* 68:89–95.

Gonoi, T., and B. Hille. 1987. Gating of Na Channels. Inactivation modifiers discriminate among models. *J. Gen. Physiol.* 89:253–274.

Hamill, O. P., A. Marty, E. Neher, B. Sakmann, and F. J. Sigworth. 1981. Improved patch clamp techniques for high-resolution current recording from cells and cell-free membrane patches. *Pflugers Arch.* 391:85–100.

Herrington, J., C. R. Solaro, A. Neely, and C. J. Lingle. 1995. Suppression of calcium- and voltage-activated current by muscarinic acetylcholine receptor activation in rat chromaffin cells. *J. Physiol. (Lond.).* 485: 297–318.

Hodgkin, A. L., and A. F. Huxley. 1952. A quantitative description of membrane current and its application to conduction and excitation in nerve. *J. Physiol. (Lond.).* 117:500–544.

Horn, R., and A. Marty. 1988. Muscarinic activation of ionic currents measured by a new whole-cell recording method. *J. Gen. Physiol.* 92:145–159.

Isacoff, E. Y., Y. N. Jan, and L. Y. Jan. 1990. Evidence for the formation of heteromultimeric potassium channels in Xenopus oocytes. *Nature.* 345:530–534.

Kilpatrick, D. L., F. H. Ledbetter, K. A. Carson, A. G. Kirshner, R. Slepetis, and N. Kirshner. 1980. Stability of bovine adrenal medulla cells in culture. *J. Neurochem.* 35:679–692.

Knaus, H. G., A. Eberhart, G. J. Kaczorowski, and M. L. Garcia. 1994a. Covalent attachment of charybdotoxin to the β-subunit of the high-conductance Ca^{2+}-activated K^+ channel. *J. Biol. Chem.* 269: 23336–23341.

Knaus, H. G., M. Garcia-Calvo, G. J. Kaczorowski, and M. L. Garcia. 1994b. Subunit composition of the high conductance calcium-activated potassium channel from smooth muscle, a representative of the mSlo and slowpoke family of potassium channels. *J. Biol. Chem.* 269:3921–3924.

Kuo, C-C., and B. P. Bean. 1994. Na^+ channels must deactivate to recover from inactivation. *Neuron.* 12:819–829.

Lancaster, B., and P. Pennefather. 1987. Potassium currents evoked by brief depolarizations in bull-frog sympathetic ganglion cells. *J. Physiol.* 387:519–548.

Li, M., Y. N. Jan, and L. Y. Jan. 1992. Specification of subunit assembly by the hydrophilic amino-terminal domain of the *Shaker* potassium channel. *Science.* 257:1225–1230.

Lingle, C. J., C. R. Solaro, M. Prakriya, and J. P. Ding. 1996. Calcium-activated potassium channels in adrenal chromaffin cells. *In* Ion Channels, Vol. 4. T. Narahashi, editor. Plenum Press, New York.

Livett, B. G. 1984. Adrenal medullary chromaffin cells in vitro. *Physiol. Rev.* 64:1103–1161.

MacKinnon, R. 1991. Determination of the subunit stoichiometry of a voltage-activated potassium channel. *Nature.* 350:232–235.

MacKinnon, R., R. W. Aldrich, and A. W. Lee. 1993. Functional stoichiometry of *Shaker* potassium channel inactivation. *Science.* 262:757–759.

Miller, C., E. Moczydlowski, R. Latorre, and M. Phillips. 1985. Charybdotoxin, a protein inhibitor of single Ca^{2+}-activated K^+ channels from mammalian skeletal muscle. *Nature.* 313:316–318.

Morales, M. J., R. C. Castellino, A. L. Crews, R. L. Rasmusson, and H. C. Strauss. 1995. A novel β subunit increases rate of inactivation of specific voltage-gated potassium channel α subunits. *J. Biol. Chem.* 270: 6272–6277.

Neely, A., and C. J. Lingle. 1992a. Two components of calcium-activated potassium current in rat adrenal chromaffin cells. *J. Physiol. (Lond.).* 453:97–131.

Neely, A., and C. J. Lingle. 1992b. Effects of muscarine on single rat adrenal chromaffin cells. *J. Physiol. (Lond.).* 453:133–166.

Pallanck, L., and B. Ganetsky. 1994. Cloning and characterization of human and mouse homologs of the *Drosophila* calcium-activated potassium channel gene, slowpoke. *Hum. Mol. Genet.* 3:1239–1243.

Park, C.-S., and C. Miller. 1992. Interaction of charybdotoxin with permeant ions inside the pore of a K^+ channels. *Neuron.* 9:307–313.

Prakriya, M., C. R. Solaro, J. P. Ding, and C. J. Lingle. 1996. $[Ca^{2+}]_i$ elevations detected by BK channels during Ca^{2+} influx and muscarine-mediated release of Ca^{2+} from intracellular stores in rat chromaffin cells. *J. Neurosci.* 16:4344–4359.

Pusch, M., and E. Neher. 1988. Rates of diffusional exchange between small cells and a measuring patch pipette. *Pflugers Arch.* 411:204–211.

Reinhart, P. H., S. Chung, and I. B. Levitan. 1989. A family of calcium-dependent potassium channels from brain. *Neuron.* 2:1031–1041.

Rettig, J., S. H. Heinemann, F. Wunder, C. Lorra, D. N. Parcej, J. O. Dolly, and O. Pongs. 1994. Inactivation properties of voltage-gated K^+ channels altered by the presence of β-subunit. *Nature.* 369:289–294.

Role, L. W., and R. L. Perlman. 1980. Purification of adrenal medullary chromaffin cells by density gradient centrifugation. *J. Neurosci. Methods.* 2:253–265.

Ruppersberg, J. P., K. H. Schroter, B. Sakmann, M. Stocker, S. Sewing, and O. Pongs. 1990. Heteromultimeric channels formed by rat brain potassium-channel proteins. *Nature.* 345:535–537

Saito, M., C. Nelson, L. Salkoff, and C. J. Lingle. 1997. A cysteine-rich domain deinfed by a novel exon in a *Slo* variant in rat adrenal chromaffin cells and PC12 cells. *J. Biol. Chem.* 272:11710–11717.

Shen, K. Z., A. Lagrutta, N. W. Davies, N. B. Standen, J. P. Adelman, and R. A. North. 1994. Tetraethylammonium block of slowpoke calcium-activated potassium channels expressed in *Xenopus* oocytes: evidence for tetrameric channel formation. *Pflugers Arch.* 426:440–445.

Sheng, M., Y. J. Liao, Y. N. Jan, and L. Y. Jan. 1993. Presynaptic A-current based on heteromultimeric K^+ channels detected in vivo. *Nature.* 365:72–75.

Solaro, C. R., J. P. Ding, Z. W. Li, and C. J. Lingle. 1997. The cytosolic inactivation domains of BK_i channels in rat chromaffin cells do not behave like simple, open channel blockers. *Biophys. J.* 73:819–830.

Solaro, C. R., and C. J. Lingle. 1992. Trypsin-sensitive, rapid inactivation of a calcium-activated potassium channel. *Science.* 257:1694–1698.

Solaro, C. R., M. Prakriya, J. P. Ding, and C. J. Lingle. 1995. Inactivating and non-inactivating Ca^{2+} and voltage-dependent K^+ current in rat adrenal chromaffin cells. *J. Neurosci.* 15:6110–6123.

Stampe, R., L. Kolmakova-Partensky, and C. Miller. 1994. Intimation of K^+ channel structure from a complete functional map of the molecular surface of charybdotoxin. *Biochemistry.* 33:443–450.

Tseng-Crank, J., C. D. Foster, J. D. Krause, R. Mertz, N. Godinot, T. J. DeChiara, and P. H. Reinhart. 1994. Cloning, expression, and distribution of functionally distinct Ca^{2+}-activated K^+ channel isoforms from human brain. *Neuron.* 13:1315–1330.

Wang, H., D. D. Kunkel, T. M. Martin, P. A. Schwartzkroin, and B. L. Tempel. 1993. Heteromultimeric K^+ channels in terminal and juxtaparanodal regions of neurons. *Nature.* 365:75–79.

Wu, Y.-C., J. J. Art, M. B. Goodman, and R. Fettiplace. 1995. A kinetic description of the calcium-activated potassium channel and its application to electrical tuning of hair cells. *Prog. Biophys. Mol. Biol.* 63: 131–158.

Wu, Y.-C., and R. Fettiplace. 1996. A developmental model for generating frequency maps in the reptilian and avian cochleas. *Biophys. J.* 70: 2557–2570.